Article:
Di Napoli, R, Aiuppa, A, Bergsson, B et al. (2016) Reaction path models of magmatic gas scrubbing. Chemical Geology, 420. 251 - 269. ISSN: 0009-2541

https://doi.org/10.1016/j.chemgeo.2015.11.024

Reaction path models of magmatic gas scrubbing

Rossella Di Napoli [(1*)], Alessandro Aiuppa [(1,2)], Baldur Bergsson [(1,3)], Evgenia Ilyinskaya [(4)], Melissa Anne Pfeffer [(3)], Sylvía Rakel Guðjónsdóttir [(5)] and Mariano Valenza [(1)]

[(1)] Università di Palermo, DiSTeM, Palermo, Italy (*rossella.dinapoli@unipa.it),
[(2)] Istituto Nazionale di Geofisica e Vulcanologia, INGV, Sezione di Palermo, Palermo, Italy,
[(3)] Icelandic Meteorological Office, IMO, Reykjavík, Iceland,
[(4)] British Geological Survey, BGS, Nottingham, UK,
[(5)] Iceland GeoSurvey, ÍSOR, Reykjavík, Iceland

Abstract - Gas-water-rock reactions taking place within volcano-hosted hydrothermal systems scrub reactive, water-soluble species (sulfur, halogens) from the magmatic gas phase, and as such play a major control on the composition of surface gas manifestations. A number of quantitative models of magmatic gas scrubbing have been proposed in the past, but no systematic comparison of model results with observations from natural systems has been carried out, to date. Here, we present the results of novel numerical simulations, in which we initialized models of hydrothermal gas-water-rock at conditions relevant to Icelandic volcanism. We focus on Iceland as an example of a "wet" volcanic region where scrubbing is widespread. Our simulations were performed (using the EQ3/6 software package) at shallow (temperature <106°C; low-T model runs) and deep hydrothermal reservoir (200-250°C; high-T model runs) conditions. During the simulations, a high-temperature magmatic gas phase was added stepwise to an initial meteoric water, in the presence of a dissolving aquifer rock. At each step, the chemical compositions of coexisting aqueous solution and gas phase were returned by the model. The model-derived aqueous solutions have compositions that describe the maturation path of hydrothermal fluids, from immature, acidic Mg-rich waters, toward Na-Cl-rich mature hydrothermal brines. The modeled compositions are in fair agreement with measured compositions of natural thermal waters and reservoir fluids from Iceland. We additionally show that the composition of the model-generated gases is strongly temperature-dependent, and ranges from $CO_{2(g)}$-dominated (for temperatures ≤80°C) to $H_2O_{(g)}$-dominated (and more $H_2S_{(g)}$ rich) for temperatures > 100°C. We find that this range of model gas compositions reproduces well the (H_2O-CO_2-S_{TOT}) compositional range of reservoir waters and surface gas emissions in Iceland. From this validation of the model in an extreme end-member environment of high scrubbing, we conclude that EQ3/6-based reaction path

simulations offer a realistic representation of gas-water-rock interaction processes occurring underneath active magmatic-hydrothermal systems.

Keywords: magmatic gas scrubbing; gas-water-rock interaction; EQ3/6; hydrothermal systems; Iceland

1. INTRODUCTION

A recurrent, but sometimes overlooked, control factor on the chemistry of volcanic gas emissions is the interaction between magmatic gases and groundwater/hydrothermal systems. This process, commonly referred as *magmatic scrubbing* (Symonds et al., 2001), takes place as rising magmatic gases encounter any aquifer interposed between the source magma stored at depth and the surface. The resulting gas-water-rock interactions cause partitioning of water-soluble species (S, halogens) into aqueous solutions, and irreversibly modify the composition of the primary magmatic gas phase. Quantitative assessment of scrubbing is, therefore, essential for interpreting mechanisms and evolution of volcanic-hydrothermal unrests (Doukas and Gerlach, 1995; Gerlach et al., 2008; Ilyinskaya et al., 2015; Symonds et al., 2001, 2003; Werner et al., 2008, 2012; Shinohara et al., 2015). The mechanism of magmatic gas scrubbing by hydrothermal systems was introduced in the fifties (White, 1957), but it was only in the 1990s that scrubbing was invoked as a most important process to explain the anomalous low fluxes of magmatic SO_2 and HCl observed at many volcanoes worldwide, both before and after eruptions (Doukas and Gerlach, 1995; Reed, 1997). Quantitative modeling of magmatic gas scrubbing started with Symonds et al. in 2001. By using the reaction path modeling approach and the CHILLER (Reed, 1982, 1998; Spycher and Reed, 1988) and GASWORKS (Symonds and Reed, 1993) programs, the Authors numerically investigated scrubbing at shallow- and deep-water conditions, by simulating the injection of increasing amounts of a magmatic gas (T = 915°C) to aqueous solutions (ranging from diluted meteoric water and to hydrothermal solutions), in the 0.1-5 MPa pressure range. Results of these simulations highlighted the large impact of scrubbing on the chemistry (abundance of $SO_{2(g)}$, $HCl_{(g)}$, $HF_{(g)}$ and, to a minor extent, $CO_{2(g)}$ and $H_2S_{(g)}$) of volcanic gases. Symonds et al. (2001) also discussed the implications of scrubbing for volcano monitoring, and concluded that volcanic emissions of $SO_{2(g)}$ and $HCl_{(g)}$ are essentially reduced when scrubbing occurs. In such conditions, $CO_{2(g)}$ remains the most useful magmatic gas species to be monitored, until interactions between magmatic gas and hydrothermal aquifers are eluded by opening of a dry degassing pathway to the surface, shortly prior to or during a volcanic eruption. More recently, Marini and Gambardella (2005) first tested the ability of the EQ3/6 software package to model the irreversible gas mass exchanges occurring during addition of

magmatic gas to pure water, at near-surface conditions (0.1 MPa). The obtained results were qualitatively similar to those of Symonds et al. (2001), confirming utility and flexibility of EQ3/6 for scrubbing calculations. More recent applications of EQ3/6 were presented in Di Napoli et al. (2013) and Ilyinskaya et al. (2015).

In spite of the major advance reached in past studies, application of thermodynamics models to scrubbing have not yet been validated using measured (natural) gas compositions. In this paper, we apply the reaction path modeling approach (Helgeson, 1968) with the specific objective of quantitatively investigating magmatic gas scrubbing at two volcanoes exhibiting extensive scrubbing: Hekla volcano and the Krýsuvík volcanic system, both in Iceland (Hk and Kr in Figure 1). These case studies are here taken as archetypes of systems in which gas-water-rock interactions proceed in shallow and deep-reservoir hydrothermal environments, respectively. So doing, we provide more theoretical and observational confirmation to our initial attempts to model magmatic gas scrubbing at Icelandic volcanoes (Ilyinskaya et al., 2015) and, even more importantly, extend these to higher-temperature hydrothermal interactions. The large mass of previous work on hydrothermal systems has clearly demonstrated that compositions of surface hydrothermal manifestations are controlled by a variety of processes, occurring at both deep reservoir conditions (e.g., fluid-mineral reactions; Arnórsson et al., 1983; Giggenbach, 1981, 1988; Reed and Spycher, 1984; Stefánsson and Arnórsson, 2000, 2002) and upon ascent of fluids from the reservoir to surface (e.g., boiling, degassing, mixing, oxidation and further water-rock interactions; Arnórsson, 1985; Arnórsson et al., 2007; Fournier, 1989; Kaasalainen and Stefánsson, 2012; Markússon and Stefánsson, 2011; Nordstrom et al., 2009). In comparison to these well characterised processes, the interaction mechanisms (scrubbing) of magmatic volatiles inside hydrothermal reservoirs have received less attention so far, and motivate the present study. We ultimately demonstrate that EQ3/6 scrubbing models satisfactorily reproduce the chemical compositions of cold (Hekla-type) natural gas emissions and, when combined with other processes such as boiling, of the near-boiling hydrothermal steam vents in Iceland. We also find good match betwenn our model fluids and compositions of reservoir fluids in boreholes. Our developed model approach, after the validation study described here, can now generically be used to investigate scrubbing process at any volcano worldwide.

2. MATERIALS AND METHODS

2.1 EQ3/6 code

Reaction path models of magmatic gas scrubbing are here carried out by means of EQ3/6 (version 7.0; Daveler and Wolery, 1992; Wolery, 1979, 1992a, 1992b; Wolery and Daveler, 1992),

a software package combining together the EQ3NR and EQ6 codes (see Appendices A and B). By using thermodynamic and kinetic constraints, this software performs numerical simulations of aqueous solutions that evolve, through a set of irreversible (not at equilibrium) reactions, towards a final equilibrium state. The reaction progress variable (ξ) (Helgeson, 1968) describes the extent to which reactions have progressed.

2.2 Range of conditions investigated by EQ3/6 reaction path modeling

Scrubbing of a high-temperature magmatic gas at hydrothermal or shallow groundwater conditions is simulated by EQ3/6 via the stepwise addition of a deep magmatic gas (*initial gas*) to 1 kg of a *starting aqueous solution*, in contact with reservoir rocks (*solid reactants*) (Table 1 and Figure 2). The initialization of the model runs is described in Appendices A and B. The model input parameters are listed in Tables 1-2 and A.1.

We investigated scrubbing at temperatures of ≤106°C (low-T model runs; Table 2) and 200-250°C (high-T model runs; Table 2), in the attempt to compare our modelling results with natural gas compositions from respectively low-T (e.g., Hekla volcano) and higher-T (e.g., Krýsuvík) volcanic/hydrothermal systems. The low-T model runs are an extension-implementation of those presented in Ilyinskaya et al. (2015): a wider range of gas/water ratios is explored and, more importantly, $HCl_{(g)}$ is now incorporated in the model. The high-T runs are first presented in this study.

A total of 8 different model run types (A-H) were performed (Table 2). Low-T run types (A to D in Table 2) consisted each of 5 to 11 runs (e.g., A_1, A_2, etc.), which corresponded to distinct steps (0.6-1.5 moles each) of gas addition to a *starting aqueous solution* (see Section 4 and Figure 2). Similarly, seven runs (e.g., seven iterative additions of 0.3 mol gas each) were performed in each of the high-T run types (E to H; Table 2).

2.3 Degassing calculations

EQ3/6 code does not implement any routine to perform degassing calculations. We therefore used an independent calculation routine to (*i*) extract from EQ6 the model aqueous solutions, (*ii*) calculate for each of them the total gas pressure $Pgas_{TOT}$ (where $Pgas_{TOT} = P_{H_2O} + P_{CO_2} + P_{H_2S} + \ldots$) (Figure 5), and *(iii)* process any gas over-saturated solution (where $Pgas_{TOT} > P_{run}$) in a single-step degassing process (Henley et al., 1984), to release the excess dissolved gas until attainment of an equilibrium condition ($Pgas_{TOT} = P_{run}$) (Figure 2 and Table 2). In brief, from the molar fractions of each j-*th* gas species in the *un-degassed aqueous solution* ($(n_j/n_{H2O})_i$) (*aqueous solution_n* in Figure 2), extracted from the EQ6 output file, we calculated the gas molar fractions in the *degassed*

aqueous solution_n ($(n_j/n_{H2O})_{lq}$) and in the *separated gas phase_n* ($(n_j/n_{H2O})_g$) (see Figure 2), using Equations 1-2:

$$\left(\frac{n_j}{n_{H_2O}}\right)_{lq} = \left(\frac{n_j}{n_{H_2O}}\right)_i \cdot \left(\frac{1}{B_j \cdot f + 1 - f}\right) \quad (1)$$

$$\left(\frac{n_j}{n_{H_2O}}\right)_g = \left[\left(\frac{n_j}{n_{H_2O}}\right)_i - \left(\frac{n_j}{n_{H_2O}}\right)_{lq} \cdot (1-f)\right] \div f \quad (2)$$

where f is the degassing fraction, and (B_j) the partition coefficient of each gas, calculated at the run temperature (T_{run}) using the relations of Giggenbach (1980). The value of f was interactively changed until Equation 3 was satisfied:

$$P_{gas_{TOT}} = \sum_j \left(\frac{n_j}{n_{H_2O}}\right)_{lq} \cdot K_{Hj} = P_{run}\ (\text{at}\ T_{run}) \quad (3)$$

where $Pgas_{TOT}$ is total pressure (as sum of partial pressure values of all j-*th* gas species) of *degassed aqueous solution*, $(n_j/n_{H2O})_{lq}$ (derived from Eq.1) and K_{Hj} are the molar fractions and the Henry's constant of j-*th* gas specie in *degassed aqueous solution*, respectively, and P_{run} is the run pressure. P_{run} was taken constant at 1.013bar for T<100°C runs, and equaled the water saturation pressure at the simulation-run temperature (T_{run}) in high-T (200-250°C) runs (Table 2).

3. BACKGROUND

3.1 Hekla and Krýsuvík

Hekla (Figure 1) is one of the most active and frequently erupting volcanoes in Iceland (Höskuldsson et al., 2007; Larsen et al., 1999), but the compositional signature of its magmatic gases, its magmatic gas output, and the structure of its magmatic-hydrothermal system, all remain very poorly known. This paucity of information reflects the absence of sustained gas vent emissions during quiescent intervals; consequently, degassing at Hekla has long been only indirectly investigated through analysis of groundwaters issuing at the base of the volcano (Flaathen and Gíslason, 2007; Flaathen et al., 2009; Gíslason et al., 1992). Warm (40-70 °C), diffuse degassing on the volcano's summit emits ~14 tons of CO_2-dominated volcanic gas/ day (Ilyinskaya et al., 2015). The Authors identified a magmatic origin for this gas based on C isotopes, and preliminary reaction path modeling suggested that these CO_2-rich (S-poor) fluids may be the result of extensive scrubbing of deeply sourced magmatic volatiles into the Hekla groundwater system.

The Krýsuvík geothermal area (Arnórsson, 1987), in the Reykjanes Peninsula (Figure 1a), is the surface expression of one of the several active hydrothermal systems in Iceland (Arnórsson, 1995). Thermal manifestations include steam-heated hot springs and mud pools, extensive acid surface alteration, and steaming hot grounds (Markússon and Stefánsson, 2011). In the geothermal reservoir, being <1000m deep (Arnórsson et al., 1975) and 200-300°C in temperature (Arnórsson,

1987; Arnórsson and Gunnlaugsson 1985; Poreda et al., 1992), the recharge meteoric fluids (with some minimal seawater contributions) react with host rock minerals in the presence of a deeply sourced (possibly magmatic) gas phase, acquiring the characteristic NaCl-composition of fully equilibrated hydrothermal brines (Arnórsson et al 2007; Giggenbach, 1988). Upon depressurization along faults and fractures, these reservoir fluids boil to produce the geothermal steams feeding the surface (~100°C) fumaroles (Arnórsson, 1995; Guðjónsdóttir, 2014; Poreda et al., 1992). These rising steams, upon shallow condensation, and oxidation of H_2S to H_2SO_4, lead to intensive acidic alteration and to formation of SO_4-rich steam-heated springs and pools (Markússon and Stefánsson, 2011).

3.2 The natural gas dataset

Iceland is an ideal location to study gas-water-rock interactions because of widespread volcanic and geothermal activity in the presence of huge groundwater circulation. We use this end-member environment to validate the use of our EQ3/6 models for simulating magmatic gas scrubbing at natural conditions. Although our models were specifically initialised (Tables 1-2) at conditions suitable for Hekla volcano and the Krýsuvík geothermal system, that are respectively examples of gas-water-rock reactions at shallow (<100°C) and deep-reservoir (200-250°C) conditions, we extend our model vs. natural sample comparison to volcanic gases released from the 26 active volcano/hydrothermal systems in Iceland (Figure 1b and Table 3).

The complex interactions between the Mid-Atlantic Ridge and an underlying mantle plume have controlled the location of volcanism in Iceland (Figure 1a): due to the westward American-Eurasian plate boundary migration, relative to the stable Icelandic hotspot, volcanic activity has progressively migrated eastward (Garcia et al., 2003; Ward, 1971; Saemundsson, 1974), from the West Volcanic Zones (>3 Myr; Garcia et al., 2003) towards the today active rifts of the North and the East Volcanic Zones, hosting the currently most active volcanic systems (Figure 1a). The volcanic gases in our dataset (Table 3) include samples from both West and East-North Icelandic Volcanic Zones (Figure 1a). Their isotopic features (Arnórsson, 1986; Arnórsson and Barnes, 1983), with their magmatic $\delta^{13}C_{(CO2)}$ of ~ -2.5 to -4‰ (Barry et al., 2014; Marty et al., 1991; Poreda et al., 1992), and the $^3He/^4He$ isotopic ratios higher than MORB (from 8.5 to 20 Ra; Poreda et al., 1992), reflect well the strong deep-mantle plume imprint.

The natural gas compositions listed in Table 3 are based upon a review of published, data of hydrothermal fumaroles and near-vent plumes in Iceland. This compilation has been extended with the results of new unpublished gas measurements (El, Gr in Table 3), obtained during field campaigns made for volcano monitoring at the Icelandic Meteorological Office within the context

of the EU-FP7 project "*Futurevolc*" with a portable Multi-component Gas Analyzer System (Multi-GAS; Aiuppa et al., 2005). We additionally list in Table 3 the compositions of well fluids (well steam, "WS", and dissolved gases in reservoir waters, "WW") collected from geothermal boreholes at depth (data source: Ármannsson et al. 1982; Arnórsson, 1986; Arnórsson and Gunnlaugsson 1985; Arnórsson et al., 1975; Bjarnason, 2000; Guðmundsson et al., 1975). These borehole data provide constraints on reservoir fluid composition, prior to decompression boiling, and are therefore very useful independent tests for the validity of our model outputs.

In the H_2O/10-CO_2-5S_{TOT} triangular plot of Figure 1b, the natural gas samples (Table 3) fall into three distinct compositional domains. The majority of the samples are the near-to-boiling steam vents/fumaroles, corresponding to the surface discharges of high-temperature (T>180°C), volcano-hosted hydrothermal reservoirs. These samples are identified as "hydrothermal gases" in Figure 1b. Although a magmatic origin (from a MORB-mantle plume mixture) is implicated for both CO_2 and noble gases, based on isotopic data (Barry et al., 2014; Ilyinskaya et al., 2015; Kurtz et al., 1985; Macpherson et al., 2005; Polak et al., 1976; Poreda et al., 1980, 1986, 1992), these gas samples show clear signs of hydrothermal derivation of the emitted fluids, including (Figure 1b): *(i)* very high H_2O/CO_2 ratios (often > 100 and up to 630), *(ii)* very low total sulfur contents (S_{TOT} < 0.3 % vol; CO_2/S_{TOT} 1.9 - 61450), and *(iii)* dominance of H_2S over SO_2 (typically below detection). Data from the Krýsuvík geothermal system (Arnórsson, 1986, 1987; Arnórsson and Gunnlaugsson, 1985; Guðjónsdóttir, 2014) clearly fall into this category of H_2O-rich hydrothermal steam samples (Figure 1b). These compositions overall imply that vigorous interaction (re-equilibration) of magmatic fluids within hydrothermal reservoirs must have occurred (Arnórsson, 1983, 1986; Arnórsson and Gunnlaugsson, 1985; Barth, 1950; Sigvaldason, 1966). The very low sulfur concentrations, in particular, reflect extensive magmatic gas scrubbing at hydrothermal reservoir conditions (Arnórsson, 1986; Arnórsson and Barnes, 1983; Arnórsson and Gunnlaugsson, 1985; Ilyinskaya et al., 2015; Oskarsson, 1984). Deep-reservoir well fluids (WW and WS in Table 3), collected from geothermal boreholes at depth, also share similar H_2O-rich and S-poor compositions (Arnórsson and Gunnlaugsson, 1985).

A second group of "cold gases" (Figure 1b) essentially correspond to gas samples from Hekla volcano; these exhibit unusually CO_2-rich compositions (H_2O/CO_2 of 1.2±1.4), that have been interpreted (Ilyinskaya et al. 2015) as reflecting even larger extents of magmatic gas scrubbing, occurring in a lower-temperature (< 100 °C) groundwater environment.

Finally, "magmatic gases" are characterized by much higher S_{TOT} (>3% vol.), lower CO_2/S_{TOT} (from 1.1 to 5) and H_2O/CO_2 (as low as 5; Table 3) ratios relative to hydrothermal steam samples, and prevalence of SO_2 over H_2S. Information on the chemistry of high-temperature magmatic gas

emissions in Iceland is limited, and includes measurements made during only three volcanic eruptions (Surtsey in 1963 from Sigvaldson and Ellison, 1968; Eyjafjallajökull/Fimmvörduháls in 2010 from Burton et al., 2010; and Bárðarbunga/Holuhraun in 2014-2015 from Burton et al., 2014; Gíslason et al., 2015; Pfeffer et al., 2015) (Table 3). Note that some of the most H_2O-rich gases emitted during the early stages of the Bárðarbunga/Holuhraun eruption (Figure 1b) have been interpreted to reflect some extent of meteoric water entrainment in the plume (measured by the Multi-GAS) (Gíslason et al., 2015).

4. MODELS OF MAGMATIC SCRUBBING: SEQUENCE OF COMPUTATIONAL OPERATIONS

In order to explore scrubbing at different T-P conditions, we combined reaction path models (Sections 2.1, 2.2 and Appendices A and B) with degassing calculations (Section 2.3), to finally derive the chemical composition of both aqueous and gas phases formed after reaction of magmatic gases with hydrothermal solutions and host rock.

The typical sequence of computational operations is illustrated in Figure 2. For a given *model run* type (e.g. "A_1-11*"* in Table 2), several distinct runs were carried out (see *number of runs* in Table 2). At the first simulation run, *Run_1* in Figure 2 (e.g. A_1 run in Table 2), n_{g,run_1} moles of *initial gas* (T_g = 800 °C; Table 1) are added to 1kg of *initial aqueous solution* (T_w = 4.1 °C; Table 1) while n_s moles of *solid reactant* are available to dissolve (see also Table 2). The temperature of the run T_{run_1} (Figure 2) is either derived by enthalpy balance (for low-T model runs; see Appendix A) or a-priori fixed to fit geothermal reservoir temperatures (for high-T model runs).

During the EQ6 model reaction path, gas and solids dissolve (at their specific rates; see Appendix A) and secondary solid phases precipitate (if reaching over-saturation). At the end of the run, EQ6 returns the chemical composition of a new aqueous solution (*aqueous solution_1*; Figure 2) that, due to dissolution of the *initial gas*, has higher gas content than the *initial aqueous solution* (Figure 2). If a state of over-pressurization ($Pgas_{TOT} > P_{run}$) is reached, the excess gas is separated to a gas phase by single-step degassing, until a new equilibrium is attained ($Pgas_{TOT} = P_{run}$) (Section 2.3). The chemical compositions of the released gas phase (*separated gas phase*_1 in Figure 2) and of the degassed liquid (*degassed aqueous solution_1*; Figure 2) are then obtained, the latter being then used as *starting aqueous solution* (Figure 2) in the following simulation run (*Run_2*; Figure 2).

In *Run_2* of the same model run type, n_{g,run_2} moles of *initial gas* (see also n_{g,run_n}, in Table 2) are added to the *starting aqueous solution* (the *solid reactant* is kept at same amount as in *Run_1*; see also Table 2). The new reaction path calculations carried out in *Run_2* (e.g. A_2 run in Table 2) occur at temperature T_{run_2}. At the end of this run, *aqueous solution_2* is outputted by EQ6, which is

again degassed in a single-step degassing (at T_{run_2}) in order to derive *degassed aqueous solution_2* and *separated gas phase_2* (in Figure 2). Each EQ6 run simulation is run out until a target temperature is reached (see Appendix A).

5. MODELING RESULTS

We report results for 8 different model run types, which we use to explore magmatic gas scrubbing at different P, T conditions. As summarized in Table 2, all runs of a given type (e.g., A_1 to A_11; Table 2) are initialized with identical input parameters (*initial gas*, *solid reactants*), except for the amount of *initial gas* added to the *starting aqueous solution* (Figure 2 and Table 2).

Run types A to D (Table 2) are all designed to investigate reaction paths in the 14 to 106°C temperature range, but are conducted using different (relative) gas dissolution rates (Table 2; see Appendix A); these low-T model runs aim therefore at investigating scrubbing in shallow groundwater conditions.

Run types E to H (high-T model runs; Table 2) are executed at temperatures of either 200 or 250°C, to explore the effect of scrubbing at hydrothermal reservoir conditions.

The same *initial aqueous solution* (Holm et al., 2010) and *initial gas* (Burton et al., 2010) (Table 1) are used throughout. We initialise our simulations with two distinct *solid reactants*, a basaltic glass from Hekla (model runs B-D; Table 2) and a basaltic glass from the Krýsuvík geothermal field (model runs E-H; Table 2) (Table 1). The total amount of solid reactants available to dissolve in each run (Table 2) were based on inter-granular porosities, and assuming pore spaces of the solid reactant are water-saturated (See Appendix A). Only minor fractions of the available rock is actually dissolved at the end of the runs (<2.85 and <0.35 moles at 200° and 250° C, respectively; Table 2). Model runs A_1-11 (Table 2) are conducted in the absence of *solid reactant* to explore scrubbing in a simple gas-water system. More details on the initialization of the runs are given in Appendix A.

5.1 Aqueous solutions

Figures 3-4 illustrate some selected results of our model simulations. These Figures demonstrate, in particular, the physical-chemical properties and chemical compositions of the model *aqueous solutions* (*aqueous solution_n* in Figure 2). We identify with circles model aqueous solutions derived from low-T (A-D) model runs, while stars represent aqueous solutions from high-T (E-H) model runs.

The model evolution of pH in the *aqueous solutions* is illustrated in Figure 3a. In the low-T model run, the pH of model *aqueous solutions* decreases as increasing amounts of *initial gas* are

stepwise added to the system. The model *aqueous solutions* are far more acidic (pH<4) than the *initial aqueous solution* (blue square in Figure 3a), reflecting the dissolution of acidic magmatic gases. Model runs A_1-11, in which no *solid reactants* has been made available to interact with the *starting aqueous solution* (see Table 2), produce *aqueous solutions* that are more acidic (pH from 2 to 1) than those obtained in model runs B-D (pH from 4 to 2). In contrast, neutral to basic (pH of ~7.8-8.5) *aqueous solutions* are obtained at temperatures of 200 and 250°C (E-H model runs; Table 2), due to the increased buffering role of dissolving *solid reactants*.

Likewise pH, the redox conditions of our model *aqueous solutions* also exhibit drastic modifications (Figure 3b) in consequence of gas-water-rock interactions. While in high-T model runs the oxygen fugacity (expressed as Log f_{O2}) was externally fixed by the empirical relation of D'Amore and Panichi (1980), this parameter was left free to vary during the low-T simulation runs. In these latter cases, very reducing redox conditions (Log f_{O2} ~ -70) are seen in response to the first addition (*run_1*; Figure 2) of magmatic gas (*initial gas*) to the *initial aqueous solution* (initial Logf_{O2} = -0.6) (see Figure 3b). Afterwards, along the sequence of simulation runs (of a given model run type), the Log f_{O2} of *aqueous solutions* progressively increases with temperature, up to Log f_{O2} ~ -47 at 106°C. This model evolution falls closely to the theoretical curve predicted by the H_2S-SO_2 redox buffer of Giggenbach (1987).

The chemistry of the *aqueous solutions* also evolves along the model reaction paths (Figure 4). The relative abundances of major dissolved anions (Figure 4a) and cations (Figure 4b), in particular, exhibit substantial chemical modifications in response to the progressive addition of magmatic gas to aqueous solutions. In low-T model runs, as exemplified in Figure 4a by run D_1-5, model solutions evolve along a compositional trend, from the carbon-dominated composition of the *initial aqueous solution* (blue square) towards compositions enriched in sulphur ($S_{TOT} = S^- + SO_4^{2-}$) and, to a minor extent, chlorine (as Cl^-) (Figure 4a). Overall, this compositional evolution reflects the rapid response of *aqueous solution* chemistry to dissolution of the S-Cl-rich *initial gas*. In contrast, in the same temperature range (from 14 to 106°C), no evident change is observed in dissolved cations (Figure 4b): all modelled *aqueous solutions* plot in the proximity of the Mg corner, and overlap with the composition of the *initial aqueous solution*.

Results of the high-T model runs highlight that the addition of the *initial gas* at 200°C and 250°C guides the model reaction paths towards net relative enrichments in dissolved Cl (see stars in Figure 4a) at the expenses of sulphur and carbon. The latter are essentially removed by precipitation of S- (pyrite) and C-rich (carbonates) secondary minerals from model solutions at neutral to basic pHs. In terms of dissolved cations, 200-250°C modelled solutions have compositions that contrast with those obtained in low-T model runs. The high-T *aqueous solutions* exhibit the characteristic

Mg-depletion trend, and alkali enrichment patter, that is typical of "mature" hydrothermal fluids having progressed towards a state of equilibrium (Giggenbach, 1988). Our modelled Na/K ratios (see stars in Figure 4b), in particular, are well consistent with those predicted at full-equilibrium conditions at run temperatures (as given by the full equilibrium line of Giggenbach, 1988).

5.2 Gas phase

The model-predicted evolution of gas phase composition is shown in Figures 5-6.

In the low-T runs (A-D; Table 2), the model *aqueous solutions* reach over-saturation ($Pgas_{TOT} > P_{run}$) after addition of ~0.6 moles of gas (e.g., at ~14 °C) (Figure 5). For all the runs at T> 14°C, we calculate therefore the model evolution of the *separated gas phase*, e.g. the gas phase obtained after single-step degassing of the over-pressurized aqueous solutions formed by interaction with the *initial gas* (Section 2.3). Figure 6 shows these compositions, and demonstrates that these are manifestly dominated by $CO_{2(g)}$ (from 97 to 74% in vol.) for temperatures ≤80°C; at higher temperatures (80-106°C), water vapor exceeds $CO_{2(g)}$ to become the main gas species ($H_2O_{(g)}$ = 60 – 85 vol. %) (Figure 6). $H_2S_{(g)}$ and $HCl_{(g)}$ are minor constituents of the modeled *separated gas phase* over the entire 14-106°C temperature range (Figure 6). At all (T < 106°C) conditions explored, $H_2S_{(g)}$ and $HCl_{(g)}$ concentrations increase with increasing temperatures, implying more effective gas phase transport of both species in gas-rich environments. In contrast to $CO_{2(g)}$ and $H_2O_{(g)}$, which exhibit overlapping trends for all low-T (A-D) run types, $H_2S_{(g)}$ and $HCl_{(g)}$ appear more sensitive to the conditions at which model runs are conducted (see Table 2). For examples, $HCl_{(g)}$ concentrations are substantially different depending on if a solid reactant is present or absent in the simulation runs (Figure 6): model run type A (Table 2), in which the solid reactant is not present, outputs modeled $HCl_{(g)}$ concentrations that are more than one order of magnitude larger than obtained (at same temperature) in model run types B-D (*solid reactants* present; Table 2). Clearly, $HCl_{(g)}$ is more effectively transported in the gas phase in the extremely acidic conditions (Figure 3) that prevail in the solid reactant-free run. Similarly, the different input conditions of model run types (Table 2) lead to subtle (but still appreciable) variations in $H_2S_{(g)}$ concentrations (Figure 6). A comparison of results of model runs types B-D, all made using the same input *solid reactants* (Table 2), shows that (at any given temperature), the $H_2S_{(g)}$-richest gas is obtained where the gas dissolution rate is higher (26 times rock dissolution rate, model runs D; Table 2).

In the high-T run types (E-H), gas over-saturation is reached after ~0.2 (200 °C) to ~0.8 (250 °C) moles of gas are added to 1 kg of *initial aqueous solution* (Figure 5). In the gas-poor regime, e.g. below the saturation threshold (of 0.2-0.8 moles), all gas added to model *aqueous solutions* remains in dissolved form. At higher gas contents, e.g. above the saturation threshold (>0.2 or >0.8

moles), gas species partition between the aqueous solutions and a free vapor phase. In this latter case, the gas-phase composition of coexisting aqueous and vapor phase is computed (by single-step degassing, Eq. 2) and plotted in Figure 6.

The *dissolved gas* compositions of model *aqueous solutions*, at both 200 and 250°C, contain relatively small amounts of dissolved CO_2 (0.03 - 0.2 vol. %), H_2S (~ $6 \cdot 10^{-4}$ - 0.05 vol. %) and HCl (~ $8 \cdot 10^{-12}$ - $3 \cdot 10^{-8}$ vol. %). The lowest dissolved gas concentrations are of course obtained in the gas-poor model regime. The compositions of the *separated gas phases* (calculated only at conditions where a free gas-phase is formed) are also H_2O-dominated ($H_2O_{(g)}$ ~ 81-83 vol.%), but yet more rich in $CO_{2(g)}$ (~ 15 - 19 vol. %) and $H_2S_{(g)}$ (~ 0.1 - 2 vol. %) than in the gas under-saturated conditions. The neutral pH conditions of the 200-250°C model runs (Figure 3a) result in lower fractions of $HCl_{(g)}$ (from $7 \cdot 10^{-10}$ to $6 \cdot 10^{-8}$) in the *separated gas phases*, relative to 14-106°C runs (Figure 6). This model observation is consistent with $HCl_{(g)}$ being typically undetectable in hydrothermal steam samples (Chiodini and Marini, 1998).

5.3 Secondary minerals formed

A range of secondary mineral phases is allowed to form in the reaction path model runs, when/if reaching saturation in model *aqueous solutions*. Our low-T model runs predict the formation of large amounts of carbonates and pyrite, which act as sinks of carbon and sulphur from model *solutions*. In the same model runs, the minerals chalcedony, kaolinite, smectites and zeolites are formed, and therefore control abundance of Si, Al and other cations leached from the *solid reactant*. This mineral assemblage agrees well with observed alteration mineral paragenesis in low-T (<100°C) hydrothermal fields (Flaathen et al., 2009; Markússon and Stefánsson, 2011; Gysi and Stefánsson, 2011). Calcite and pyrite are also predicted to precipitate in our high-T model runs. In this 200-250°C temperature range, chalcedony is replaced by quartz and smectites by chlorite in the model secondary mineral assemblage. High-T zeolite varieties (e.g. wairakie, scolecite), albite, K-feldspar and epidote are also formed in the last stages of the reaction path of our high-T model runs. These alteration mineral assemblages, predicted by our high-T model runs, match well experimental results from Gysi and Stefánsson (2012), and are consistent with the observed distribution of hydrothermal minerals in boreholes from Krýsuvík (Arnórsson, et al., 1975) and Krafla (Ármannsson et al., 1982).

6. DISCUSSION

Quantitative models of magmatic gas scrubbing have increasingly grown in popularity in the geological literature (Marini and Gambardella, 2005; Symonds and Reed, 1993) since it became

clear that reactions between magmatic gases and aquifers play a key control on the chemistry of fluids released by quiescent volcanoes (Doukas and Gerlach, 1995; Symonds et al., 2001). However, due to the complexity of reaction pathways, and the relatively high number of unknown variables, model results have been difficult to match against natural volcanic gas compositions, and model applications to real volcano case studies have remained few in number (Di Napoli et al., 2013; Shinohara et al., 2015; Symonds et al., 2001; Werner et al., 2012).

The EQ3/6 (Daveler and Wolery, 1992; Wolery and Daveler, 1992) reaction path modelling approach (Helgeson, 1968; Helgeson et al., 1969), used here, offers a comprehensive theoretical scheme to quantitatively interpret mechanisms and pathways of the interaction between magmatic gases and meteoric/hydrothermal aqueous solutions. One major advantage offered by EQ3/6 is its flexibility, including the possibility to initialise runs with a set of input parameters including mass, chemical composition and reaction thermodynamic/kinetic data of all the involved reactants that can be adapted to real volcano conditions. In this work, we show that EQ3/6 model runs, if suitably initialised with a proper set of input parameters (Tables 1-2), generate results that are in fair agreement with measured fluid emissions (gas and thermal water) from Icelandic volcanoes.

6.1 Scrubbing in groundwater environments

Our low temperature (< 106 °C) model runs aim at quantitatively modelling scrubbing of magmatic gases at shallow groundwater conditions. The *separated gas phases* outputted by our simulations (Figure 6) correspond to the gases that would escape from aqueous solutions after they have interacted with (and have become enriched in) magmatic gases. Low-T simulations predict a range of *separated gas* compositions (Figure 6), depending on temperature, regime (high gas vs. low gas) and phase relations (gas+water vs. gas+water+rock) at which reactions occur.

To test if these models offer a realistic representation of natural conditions, we compare their results with natural gas compositions from Hekla volcano (Ilyinskaya et al., 2015). We initially test if the range of gas CO_2/S_{TOT} ratios (with $S_{TOT} = H_2S_{(g)}+SO_{2(g)}$) predicted by our low-T model runs match the compositional range of Hekla volcanic gas samples. This comparison is made in Figure 7, where the characteristic volcanic gas CO_2/S_{TOT} ratios ($\mu \pm 1\sigma$; Table 3) for several volcanic/hydrothermal systems in Iceland (including Hekla) are plotted against the corresponding discharge or deep reservoir temperature. Recent works have demonstrated a negative temperature dependence of the gas CO_2/S_{TOT} ratio in several volcanic regions, including Kamchatka (Aiuppa et al., 2012), Italy (Aiuppa et al., 2013), Chile (Tamburello et al., 2014), and Central America (Aiuppa et al., 2014). This dependence, arising from the commonly high CO_2/S_{TOT} ratios measured in cold gas samples worldwide, has been suggested to reflect the high extents of sulfur scrubbing that affect

445 the feeding magmatic gas phase at the low-temperature end of the gas population. We show (Figure 7) that Icelandic gases do not make exception to the general rule, given the very high (>10^3) CO_2/S_{TOT} ratios seen in low-T (<100°C) gas samples from Hekla and Grímsvötn (Hk and Gr in Figure 7), all well above the magmatic gas range (CO_2/S_{TOT} ratios of 1.13±0.49 (Holuhraun), 1.2±0.8 (Surtsey) and 5 (Fimmvörduháls); see Table 3).

450 Our low-T models runs (run types A-D) provide quantitative constraints in support to the scrubbing hypothesis. We find that the model-predicted CO_2/S_{TOT} ratios in the low-T (4-106 °C; run types A-D) *separated gas phases* form a compositional band, stretching along the upper-left portion of Figure 7, which perfectly overlaps with the compositions of the Icelandic cold gas samples. Our low-T model runs are designed to represent the natural condition in which magmatic gases are 455 injected into a (meteoric) groundwater system, leading to nearly complete scavenging of soluble S (and Cl) into the aqueous phase (see Figure 6). Therefore, the general agreement between model and observations confirm the conclusion (Ilyinskaya et al., 2015) that present-day Hekla gas emissions are the residual gases formed after extensive scrubbing of a deeply supplied magmatic gas phase into the volcano groundwater system. We here extend this argument to Grímsvötn (Gr in 460 Figure 7) (measurements made at the Saltarinn hydrothermal site) where compositions (similar to Hekla) point to the occurrence of compatible processes (Figure 7). We also note that gas compositions from Eldfell volcano (El in Figure 7), in spite of their high discharge temperatures (257°C; Table 3), exhibit CO_2/S_{TOT} ratios of 2603±1977 (Table 3), similar to those seen at "colder" systems (Hekla and Grímsvötn). We argue that relatively high vent temperatures at Eldfell do not 465 reflect large magmatic gas contributions (which, in light of our model results, appear instead limited), but, rather, are related to residual cooling of the recently formed (Heimaey 1973 eruption) volcanic cone.

Figure 8 extends our model vs. natural gas comparison to the H_2O-CO_2-S_{TOT} system. In the diagram, volcanic-hydrothermal gas samples from Iceland form a single compositional array, 470 extending from *(i)* the CO_2-dominated compositions of "*cold gas*" samples (Hekla and Grímsvötn) and Eldfell, to *(ii)* the low CO_2/S_{TOT} ratio compositions of "*magmatic gases*" (Surtsey, Eyjafjallajökull/Fimmvörduháls and Bárðarbunga/ Holuhraun). Hydrothermal steam samples, both from Krýsuvík and other hydrothermal areas in Iceland, exhibit intermediate CO_2/S_{TOT} ratios, and a tendency toward more H_2O-rich compositions (H_2O/CO_2 ratios of 2 to 950).

475 In Figure 8a, the model predicted H_2O/CO_2 vs. CO_2/S_{TOT} compositions of low-T model runs (run types A-D) show very nice agreement with observed volcanic gas compositions at Hekla. They also overlap with the natural gas emissions from Eldfell, with volcanic gases emitted at Grímsvötn

being only slightly more H_2O-rich. This overall agreement provides additional confidence on our low-T model simulations.

480

6.2 Scrubbing in hydrothermal environment

High-T model runs attempt at investigating scrubbing conditions within hydrothermal systems. To validate the general applicability of the model to real (natural) conditions, we compare (in Figures 7-8) model outputs with measured reservoir (waters and steam) and surface (e.g., 485 fumaroles and steaming pools) fluids manifestations from Krýsuvík, and other Icelandic hydrothermal systems.

6.2.1 Model vs. observations: dissolved gases in reservoir fluids

Our high-T model runs (E-H; Table 3) suggest that, for low gas additions, no gas over- 490 pressure is reached (Figure 5), so that all gas is retained by model *aqueous solutions* (here reproducing *reservoir waters*) in dissolved form (*dissolved gas* in Figures 6-7). Geologically, this condition reflects the case in which magmatic gases are totally scrubbed to reservoir fluids during hydrothermal interactions. As more gas is added to the system (Figure 5), gas species are eventually partitioned between dissolved gas in the *aqueous solution* and a coexisting equilibrium gas phase. 495 This *separated gas* phase is obviously more CO_2- and H_2S-rich than the coexisting *aqueous solution* (*dissolved gas* in *reservoir water*) (Figures 6 and 8b).

The *dissolved gas* composition of our modeled solutions (Figure 6) is compared in Figures 7 and 8b with compositions of hydrothermal reservoir waters sampled in geothermal boreholes (Ármannsson et al. 1982; Arnórsson, 1986; Arnórsson and Gunnlaugsson, 1985; Arnórsson et al., 500 1975), which are obvious geological proxies for this process in nature. We find that the *dissolved gas* compositions obtained in our high-T (run types E-H) models satisfactorily reproduce the CO_2/S_{TOT} ratio range (from 2.3 to 64) of hydrothermal reservoir waters (WW in Table 3), which are intermediate between magmatic gas (1.4-5.0) and cold-gas (>10^3) compositional domains (Figure 7). Obviously, the higher temperatures concur to augmented gas-phase sulfur transport (relative to 505 CO_2, and to low-T models). More in the specific, the 250°C model predicted CO_2/S_{TOT} ratios (4-64) match well the (observed) compositions (CO_2/S_{TOT} from 4 to 92) of hydrothermal reservoir waters from Krýsuvík (Arnórsson et al., 1975; Guðmundsson et al., 1975) which reservoir temperatures (250-260°C; Arnórsson et al., 1975; Poreda et al., 1992) are in the range of model run temperatures (Figure 7).

510 The model also predicts well the range of *dissolved gas* contents of hydrothermal reservoir waters (WW in Table 3), as seen by the overlapping H_2O/CO_2 ratio compositions of model and

natural (reservoir water) fluids in Figure 8b. Good agreement is observed, in particular, between H_2O/CO_2 ratios compositions of model solutions and reservoir waters from Krafla, Námafjall, Reykjanes and Svartsengi (Figure 8a and Table 3). Overall, this nice match between modeled and natural compositions testifies for the ability of our models in reproducing real natural conditions of magmatic-hydrothermal interactions. We however find that our models apparently over-estimate (by a factor ~ 10) the gas content in Krýsuvík reservoir waters (measured H_2O/CO_2 ratios of ~ 40,000 vs. < 3600 in the modeled aqueous solutions). Although we have no unequivocal explanation for this (relatively minor) mismatch, we speculate that some artifact during field sampling of reservoir waters may be implicated, because as stated by Arnórsson et al. (1975) in his Krýsuvík study on borehole fluids "*…when the sample is released from the sampling apparatus and transferred to the sample bottle, some of the volatiles may escape, and the results….are not considered reliable with respect to these compounds (CO_2 and H_2S)*".

6.2.2 The chemistry of hydrothermal steam samples, and the effect of boiling

Our models above reproduce interactions between magmatic gases and hydrothermal waters at reservoir conditions. While such magmatic gas scrubbing reactions, followed by equilibration with host rock minerals (Arnórsson, 1995; Arnórsson et al., 1983; Giggenbach, 1988; Reed and Spycher, 1984; Stefánsson and Arnórsson, 2000, 2002), contribute to determine hydrothermal reservoir fluid compositions, surface steam discharges have instead compositions that are determined by boiling of deep reservoir fluids in the up-flow zone (see Arnórsson, 1986, 1995; Chiodini and Marini, 1998; Giggenbach, 1980, 1993). At Krýsuvík, for example, Arnórsson (1987) used the results of gas sampling surveys, combined with calculations and models, to demonstrate extensive boiling of deep reservoir fluids in their up-flow zone (fractures and faults).

In order to have boiling fully accounted for by our simulations, and therefore reproduce steam discharge compositions (Figures 8a and 8c), we used the equations of Chiodini and Marini (1998) to calculate the model compositions of gases formed by single-step boiling of our model *aqueous solutions* (see Figure 2), from their initial temperatures of 200-250°C down to 100°C. These "boiling" model lines, shown in Figure 7 and 8c, are found to perfectly overlap with the measured compositions of hydrothermal steam emissions at Krýsuvík, and at other systems in Iceland (e.g., Krafla). This nice agreement provides additional confidence on our model outputs.

6.2.3 Model vs. observations: major element water chemistry

The major element (anions/cations) compositions of reservoir and surface waters from Krýsuvík offer an independent test as for the applicability of our models to real case conditions. Our

results demonstrate that extents and modes of magmatic gas scrubbing influence the major element composition of the interacting aqueous solutions; the question arises therefore if the model-predicted water chemistry evolution path (Figures 3, 4) finds evidence in nature.

In a series of key papers, Giggenbach (1984, 1988) demonstrated that the addition of hot magmatic gases to aqueous solutions is the prevalent source of dissolved anion species (SO_4, Cl, HCO_3) to volcanic groundwaters/hydrothermal brines, in addition to dissolving hydrothermal minerals (Arnórsson, 1983; Arnórsson et al., 2007). Interaction with hot, acidic magmatic gases also creates favourable conditions for the leaching of major rock forming cations (Na, K, Ca, Mg) from host rock formations. Giggenbach (1984, 1988) also distinguished two main environments of gas-water-rock interaction: *(i)* a shallow groundwater environment, in which dissolution of magmatic/hydrothermal gases into fast circulating meteoric fluids leads to far-from-equilibrium acid leaching of host rock formations, ultimately generating thermal waters with Ca-Mg-SO_4 ("*steam-heated groundwaters*"), Ca-Mg-SO_4-Cl ("*volcanic groundwaters*"), and/or Mg-HCO_3 ("*peripheral groundwaters*") compositions, and *(ii)* a deep hydrothermal reservoir environment, in which more prolonged water residence time allows for equilibrium conditions to be reached in the gas-water-rock system, forming the so called *"mature" Na-Cl hydrothermal brines* (Giggenbach, 1988).

Figure 4 demonstrates that our model simulations reproduce well the two distinct (shallow vs. deep) environments of gas-water-rock interaction. The shallow environment of magmatic gas-water-rock interactions is reproduced well by our low-T model runs, in which the modelled *aqueous solutions* evolve toward more acidic (Figure 3a), sulphate-rich (Figure 4a) compositions, starting from the original C-rich composition of the (meteoric-derived) *initial solution*. Ca and Mg prevail among cations in these low-T model aqueous solutions (Figure 4b). Although no thermal water sample from Hekla volcano is available to compare with our model results, we still argue that our low-T modelled *aqueous solutions* well reflect the general Ca-Mg-SO_4-Cl compositional features of *volcanic groundwaters* (Giggenbach, 1988, 1993).

The high-T model runs describe a distinct evolutionary path in Figure 4a; in which, after a transient increase in S_{TOT} (due to initial dissolution of the *initial gas*), the modelled *aqueous solutions* point toward Cl-rich compositions, because of S and C scavenging by hydrothermal minerals (pyrite, calcites and phyllosilicates) as gas-water-rock interactions advance. Concurrently, the modelled *aqueous solutions* transition, from the initially Mg-rich to more alkali-rich compositions, as the reaction path progresses (Figure 4b). We conclude that our model results well reproduce the maturation path of hydrothermal fluids, from acidic, far-from-equilibrium ("*immature*" after Giggenbach, 1988) Mg-rich solutions, towards neutral (Figure 3a) Na-K-Cl

aqueous solutions (Figure 4) similar in composition to the "*mature*" hydrothermal reservoir waters found at Krýsuvík (Arnórsson et al., 1975) and elsewhere (Arnórsson et al., 1983). Importantly, we find that the Na/K ratios predicted by our model runs are not only consistent with those observed in the Krýsuvík hydrothermal reservoir samples, but also correspond to the expected Na/K ratios at full-equilibrium conditions (Giggenbach, 1988) at the run temperature.

While, based on our model results, we confirm therefore that magmatic gas scrubbing is well implicated in the generation of Na-K-Cl chemistry of hydrothermal reservoir fluids, we are well aware that additional processes, including mixing and steam condensation, contribute to governing measured water compositions at Krýsuvík (Arnórsson, 1987; Markússon and Stefánsson, 2011). For example, reservoir waters sampled in boreholes (Arnórsson et al., 1975) show a range of salinities, and a number of them are colder (Figure 3a) and more C-rich (Figure 4a), implicating that mixing with shallower, meteoric fluids is a recurrent process at depth. This process is illustrated (in Figures 3a and 4a) by families of mixing lines connecting our *initial solution* (our meteoric end-member) with model *aqueous solution*s from high-T runs. Reservoir waters find no surface expression at Krýsuvík (contrary to other hydrothermal systems, where neutral Na-Cl thermal springs are commonly encountered; Giggenbach, 1988). Instead, the majority of the surface waters at Krýsuvík are hot, acidic mud pools and springs with Ca-Mg-SO_4-dominated compositions (Markússon and Stefánsson, 2011) (see Figure 4). These acidic fluids are thought to result from shallow-level condensation of rising hydrothermal steams (Arnórsson, 1987; Arnórsson et al., 1975; Markússon and Stefánsson, 2011). We used EQ3/6 to model dissolution of a typical Krýsuvík hydrothermal steam (99.44 vol. % H_2O, 0.49 vol. % CO_2, 0.11 vol. % H_2S) into our *initial solution* (we assume the process occurs at 1.013 bar, 53-100°C and Log fO_2 = 0.8), and obtain model solutions ("*model steam-heated waters*" in Figure 4a) that agree well with measured composition. This match again confirms utility and versatility of EQ3/6 in simulation hydrothermal processes.

7. CONCLUSIONS

We have here demonstrated that EQ3/6-based reaction path modeling is a powerful tool to quantitatively explore mechanisms and pathways influencing volcanic fluids. Our numerical simulations of gas-water-rock reactions, conducted at shallow-to-deep hydrothermal conditions, generate model results that are in good quantitative agreement with measured fluid (surface and reservoir) compositions in Iceland. We conclude that scrubbing is widespread, and that the magmatic gas phase, as it travels to the surface, is variably affected by scrubbing, in either hydrothermal (high-T) or groundwater (low-T) environment, to assume the compositional features seen exhibited by hydrothermal reservoir fluids and/or surface discharges.

At hydrothermal reservoir conditions (temperatures of 200-250°C), our gas-water-rock reaction path models demonstrate that magmatic volatiles are variably (either completely or partially) scrubbed into reservoir waters. These simulations yield model *aqueous solutions* which dissolved CO_2 and H_2S contents are well consistent with those observed in natural samples (reservoir fluids sampled in boreholes). Our simulated *aqueous solutions* also have major element compositions (of Na-K-Cl type) that reflect well the hydrothermal maturation path, from "immature", acidic Mg-rich waters, to mature neutral hydrothermal reservoir brines. We also show that single-step boiling of our 200-250°C *aqueous solutions*, down to 100°C, produces modeled steam compositions that match well the observed compositional range of natural hydrothermal steam discharges, including those of Krýsuvík. We also model condensation of this hydrothermal steam into a shallow meteoric aquifer, and obtain model solutions that are compositionally similar to the *steam-heated groundwaters* found in the field at Krýsuvík (Markússon and Stefánsson, 2011).

Our low-T model runs are initialized in the attempt to simulate interaction of magmatic gases with a shallow hydrologic system, as possibly today occurring at Hekla volcano. We find that our model runs generate model gases with CO_2-dominated compositions, matching well those of the Icelandic cold gas emissions from Hekla, Grímsvötn and Eldfell.

We finally conclude that our EQ3/6-based models, once properly initialized, can open the way to investigating magmatic gas scrubbing in a variety of hydrothermal and volcanic contexts worldwide.

8. ACKNOWLEDGEMENTS

The research leading to these results has received funding from the European Community's Seventh Framework Program under Grant Agreements No. 308377 (Project FUTUREVOLC) and ERC grant agreement n 305377 (Project BRIDGE). Dr. G. Chiodini and an anonymous Reviewer are acknowledged for their insightful comments on the manuscript.

APPENDIX A

Reaction path models and their input parameters

Reaction path modelling is initialized via EQ3NR, the EQ3/6 module used to calculate speciation of the *initial aqueous solution* (see below and Table 1). This *initial aqueous solution* is then transferred to the EQ6 module to initiate the reaction path runs. The EQ6 input file also includes the compositions of gas and/or solid phases interacting with the *initial aqueous solution,* listed as *reactant* species (Table 1). The initial amounts (moles) of each different reactant (n_g and

n_s; Table 2) is also specified in the input file. The mass of *solid reactants* (n_s in Table 2) is calculated from the total volume of solids in contact with 1 kg of *initial aqueous solution*.

The EQ3/6 model simulations were initialised by fixing a priori a suite of input parameters:

(*i*) *initial aqueous solution:* this is the *starting aqueous solution* for the first run (e.g., A_1, B_1, etc.) of each run type (see Figure 2). We adopted as *initial aqueous solution* a low-salinity (Total Dissolved Solids, TDS = 300 mg/l) cold (T = 4.1 °C) water (Holm et al., 2010), which we consider as representative for the meteoric recharge of Icelandic aquifers (Table 1). In later runs (A_2, A_3, B_2, B_3…), the *starting aqueous solution* is the *degassed aqueous solution* (cfr. Section 2.3) formed in the previous run (A_1, A_2, B_1, B_2…) (see Figure 2 and Section 4). One kg of either the *initial* or *starting aqueous solution* was allowed to react with a set of reactants (gas and solids);

(*ii*) *initial gas*: the initial gas is, by definition, the high temperature magmatic gas phase that reacts with (and partially dissolves into) each *starting aqueous solution*. There are unfortunately only a few compositional reports for high-temperature magmatic gases in Iceland, implying that the deep gas supply sustaining the activity of geothermal systems in Iceland is currently poorly determined (cfr. Section 3). We here take the gas measured by Burton et al. (2010) during the March 2010 Fimmvörduháls fissure eruption of the Eyjafjallajökull volcano as a proxy for high-T magmatic gas supply in Iceland. This Fimmvörduháls gas was thus selected as *initial gas* for our models (Tables 1 and 2). We are well aware, however, that the feeding magmatic gas in Iceland can be spatially and temporally variable, and that a more hydrous magmatic gas was for example vented during the Surtsey eruption in 1963 and, more recently, during the 2014-2015 Holuhraun eruption of the Bárðarbunga volcano (Gíslason et al., 2015; Pfeffer et al., 2015). Tests made using Surtsey or Holuhraun gas as *initial gas* in our model runs outputted model gas trends qualitatively similar (only slightly more water-rich) than those presented here. The amount ($n_{g,TOT}$ and $n_{g,run}$ moles) of Fimmvörduháls *initial gas* added to the *starting aqueous solution* in each run type, and per run, is reported in Table 2.

(*iii*) *solid reactants*: two different aquifer rocks were considered in our modelling as *solid reactants* (Table 1). A basaltic andesitic glass ($SiAl_{0.31}Fe_{0.17}Mg_{0.08}Ca_{0.13}Na_{0.14}K_{0.03}O_{2.96}$; Wolff-Boenisch et al. 2004), from the 2000 eruption of Hekla (Moune et al. 2006; 2007), was used in the low-T model runs (Tables 1 and 2); since no thermodynamic data are available for the aquifer rocks at Krýsuvík geothermal system, we selected a basaltic glass from Krafla volcano ($SiAl_{0.32}Fe_{0.24}Mg_{0.17}Ca_{0.22}\ Na_{0.09}K_{0.01}O_{3.18}$; Wolff-Boenisch et al. 2004), similar in composition to Krýsuvík basalts (Markússon and Stefánsson, 2011; Peate et al., 2009), for our high-T model runs (Tables 1 and 2). Following Oelkers and Gíslason (2001), we assume that only a hydrated surface

layer (enriched in Si, Al and OH groups) of the basaltic glass equilibrates with leaching solutions. We therefore initialized our modelling using the following *solid reactants:* "*Hyd-Hekla-glass"* ($SiAl_{0.31}O_2(OH)_{0.93}$) and*"Hyd- Krýsuvík-glass"* ($SiAl_{0.32}O_2(OH)_{0.96}$) (Tables 1 and 2), which correspond to hydrated volcanic glasses of, respectively, a basaltic andesite from Hekla and a basalt from Krafla (Wolff-Boenisch et al., 2004). These reactants dissolve according to the following reactions (Eq. A1-A2):

$$Hyd\text{- }Hekla\text{ -}glass + 0.93H^+ = SiO_2 + 0.93H_2O + 0.31Al^{3+} \quad (A.1)$$

$$Hyd\text{-}Krýsuvík\text{-}glass + 0.96H^+ = SiO_2 + 0.96H_2O + 0.32Al^{3+} \quad (A.2)$$

The total amounts of *solid reactant* interacting with 1 kg of *starting aqueous solution,* listed in the EQ6 input file, were computed using effective inter-granular porosities of 0.3 (Hekla) and 0.11 (Krýsuvík; Arnórsson et al., 1975). We assume that pore spaces of the solid reactant are water-saturated, and we use densities of 2.79 g/cm^3 and 3.04 g/cm^3 for respectively *Hyd-Hekla-glass* and *Hyd-Krýsuvík-glass* (Wolff- Boenisch et al., 2004). A total of 77.26 mol of *Hyd-Hekla-glass* and 289.23 mol of *Hyd-Krýsuvík-glass* were used respectively in low-T and in high-T model runs (Table 2).

In order to include the rock-forming metals not included in the hydrated glass compositions (see Eq. A.1-A.2 and Table 1), we used two different *special reactants* (Wolery and Daveler, 1992), here referred as *Hekla-glass-cations* and *Krýsuvík-glass-cations* (Table 1). Each *special reactant* is entered in the EQ6 input file in same amount as the corresponding hydrated glass (77.26 mol of *Hekla-glass-cations* and 289.23 mol of *Krýsuvík-glass-cations*; see Table 2), and its composition is specified as moles of metals per mole of *special reactant* (see Table 1).

(*iv*) *kinetic data*: In order to allow our reaction path modeling to run in time mode, the kinetic parameters for each reactant (gas and solid) must be fixed in the input file. Kinetic parameters of dissolution-precipitation reactions are fixed by a specific rate law in the EQ6 input file. For irreversible reactions involving solid phases, the Transition State Theory (TST) rate law (Wolery and Daveler, 1992), which is a function of aqueous solution chemistry (Table A.1), was used. Consequently, the input file was implemented with the dissolution rate constant (k; mol·cm^{-2}·s^{-1}), the apparent activation energy (E_a; kcal·mol^{-1}) (Gíslason and Oelkers, 2003), and the total surface area (s; cm^2) (derived from measured BET specific surface area; Wolff-Boenisch et al., 2004) for both *Hyd-Hekla-glass* and *Hyd-Krýsuvík-glass* (see Table A.1). *Special reactants* were set to dissolve at the same rate as the corresponding *solid reactant* (relative rate equal to 1; cfr. Section 2.1) for both *Hekla-glass-cations* and *Krýsuvík-glass-cations* (Table A.1).

The *initial gas* dissolves into the aqueous solution at a rate that is unknown (as a function of parameters such as the gas flux, or the gas/water ratio etc.), but in any case faster than that of

basaltic glass (see below); in each simulation run, we therefore assumed a relative dissolution rate of the *initial gas* as being *n* times that of the *solid reactant*. A range of *n* values was explored ("*initial gas* relative dissolution rate" in Table 2).

Since rate laws are entered in the EQ6 input file, the reaction path calculations have a defined time frame (*simulations in time mode*).

(*v*) *run pressure*: in each single run (Table 2), pressure was taken as either 1.013bar (run types A-D) or as the water saturation pressure at run temperature (run types E-H).

(vi) run temperature: in the low-T runs (run types A-D), we calculated (and entered in the input file) the temperature T_{run_n} of each single run (e.g. *run_1* in Figure 2; A_1 run in Table 2) assuming enthalpy is conserved during mixing between the *starting aqueous solution* and the *initial gas*. We express the enthalpy balance as (modified from Spycher and Reed, 1988):

$$H_{s,T_{run\_n}} = H_{w,T_w} \cdot \frac{1000}{MW_w} + n_{g,run\_n} \sum_j H_{j,T_j} \cdot X_j \quad \text{(A.3)}$$

where $H_{w,Tw}$ and $1000/MW_w$ are respectively enthalpy (J/mol) and amount (mol) of *starting aqueous solution* (here assimilated to pure water) at its temperature (T_w, °C); n_{g,run_n} (mol) stands for the amount of *initial gas* added in the considered run (*n*), and $H_{j,Tj}$ and X_j are, respectively, enthalpy (J/mol) and molar fraction of the j-*th* gas species in gas phase, at *initial gas* temperature (T_j, °C).

From enthalpy $H_{s,Trun\_n}$, run temperature (T_{run_n}) was calculated as:

$$T_{run\_n} = -3 \cdot 10^{-17}\left(H_{s,Trun\_n}\right)^4 - 1 \cdot 10^{-12}\left(H_{Ts,Trun\_n}\right)^3 + 1 \cdot 10^{-8}\left(H_{Ts,Trun\_n}\right)^2 + 0.0132\, H_{Ts,Trun\_n} + 0.01 \quad \text{(A4)}$$

This relation is derived by combining the Denbigh's (1971) enthalpy equation with the heat capacity power expression, proposed by Chase (1998).

$$H_{Trun\_n} = H_{T_{triple}} + \left[a\left(T_{run\_n} - T_{T_{triple}}\right) + \frac{b}{2}\left(T^2 - T_{T_{triple}}{}^2\right) + \frac{c}{3}\left(T^3 - T_{T_{triple}}{}^3\right) + \cdots\right] \quad \text{(A.5)}$$

This temperature is used (and kept constant) during each single run simulation. As shown in Figure A.1, the temperature of the *degassed aqueous solutions* (Figure 2) (corresponding to model run temperature) increases proportionally to the amount of *initial gas* added in the model run (Table 2). The low-T run types (A-D) give rise in Figure A.1 to four overlapping model trends, that demonstrate that a total of 6.6 moles of *initial gas* are required to raise the model run temperature, from 4.1°C (the temperature of the *initial aqueous solution*; blue square in Figure A.1) to 106°C.

The high-T model runs (E-H) were operated at constant temperatures of either 200 or 250°C (Table 2). These temperatures reflect the range of reservoir temperatures estimated/measured at Krýsuvík (Arnórsson, 1987; Arnórsson and Gunnlaugsson, 1985; Arnórsson et al., 1975). The

enthalpy balance (Eq. A.3) is not used in high-T runs, because we assume conductive heating of recharge waters as they infiltrate through hot rocks formations of the hydrothermal system.

(*vii*) *redox conditions*: redox conditions in hydrothermal reservoirs are known to be controlled by reactions involving redox couples (Chiodini and Marini, 1998). In our high-T model runs (Table 2), we therefore fixed the oxygen fugacity (as Log f_{O2}) using the empirical relation proposed by D'Amore and Panichi (1980). This redox buffering control is hardly extendable to shallow groundwater systems, and oxygen fugacity was not externally fixed in our low-T model runs simulations.

APPENDIX B

Database implementation

EQ6 uses thermodynamic data from the *data0* database. Implementation of the original *data0.com.R10* (Wolery, 1992a, 1992b) database was required, in order to include the new gas and solid reactants used in our modeling. Element compositions, dissolution reactions and equilibrium constants (as log K) at different T (from 0 to 300°C) were implemented for both *initial gas* and *solid reactants* (Tables 1 and 2). Equilibrium constants (log K) of the *initial gas* dissolution reaction were derived from dissociation of pure $H_2O_{(g)}$, $CO_{2(g)}$, $SO_{2(g)}$ and $HCl_{(g)}$. For each *solid reactant* (*Hyd-Hekla-glass* and *Hyd-Krýsuvík-glass*; Table 1), we simply derived the equilibrium constants (log K) consistent with the dissolution reactions reported in Equations A.1-A.2, by summing (stoichiometrically weighted sum) the log K of amorphous silica and gibbsite hydrolysis reactions (Oelkers and Gíslason, 2001).

9. REFERENCES

Aiuppa, A., Federico, C., Giudice, G., Gurrieri, S., 2005. Chemical mapping of a fumarolic field: La Fossa Crater, Vulcano Island (Aeolian Islands, Italy). Geophys. Res. Lett., 32; doi:10.1029/2005GL023207.

Aiuppa, A., Giudice, G., Liuzzo, M., Tamburello, G., Allard, P., Calabrese, S., Chaplygin, I., McGonigle, A.J.S., Taran, Y., 2012. First volatile inventory for Gorely volcano, Kamchatka. Geophys. Res. Lett. 39.

Aiuppa, A., Tamburello, G., Di Napoli, R., Cardellini, C., Chiodini, G., Giudice, G., Grassa, F., Pedone, M., 2013. First observations of the fumarolic gas output from a restless caldera: Implications for the current period of unrest (2005–2013) at Campi Flegrei. Geochem. Geophys. Geosyst. 14, doi: 10.1002/ggge.20261.

Aiuppa, A., Robidoux, P., Tamburello, G., Condec, V., Galle, B., Avard, G., Bagnato, e., De Moor, J.M., Martínez, M., Muñóz., A., 2014. Gas measurements from the Costa Rica–Nicaragua volcanic segment suggest possible along-arc variations in volcanic gas chemistry. Earth Planet. Sci. Lett. 407, 134-147.

Ármannsson, H., Gíslason, G. and Hauksson, T., 1982. Magmatic gases in well fluids aid the mapping of flow pattern in a geothermal system. Geochim. Cosmochim. Acta 46, 167-177.

Arnórsson, S., 1983. Chemical equilibria in Icelandic geothermal systems-Implications for chemical geothermometry investigations. Geothermics, 12, 119-128.

Arnórsson, S., 1985. The use of mixing models and chemical geothermometers for estimating underground temperatures in geothermal systems. J. Volc. geotherm. Res. 23, 299-335.

Arnórsson, S., 1986. Chemistry of gases associated with geothermal activity and volcanism in Iceland: a review. J. Geophys. Res 91, 12261-12268.

Arnórsson, S., 1987. Gas chemistry of the Krýsuvík geothermal field, Iceland, with special reference to evaluation of steam condensation in upflow zones. Jökull 37, 30-47.

Arnórsson, S., 1995. Geothermal Systems in Iceland: Structure and Conceptual Models - I. High-Temperature Areas. Geothermics 24, 561-602.

Arnórsson, S., Barnes, I., 1983. The nature of carbon dioxide waters in Snaefellsnes, western Iceland. Geothermics, 12, 171-176.

Arnórsson, S., Gunnlaugsson, E., 1985. New gas geothermometers for geothermal exploration-Calibration and application. Geochim. Cosmochim. Acta. 49, 1307-1325.

Arnórsson, S., Gunnlaugsson, E., Svavarsson, H., 1983. The chemistry of geothermal waters in Iceland, II. Mineral equilibria and independent variables controlling water compositions. Geochim. Cosmochim. Acta, 47, 547-566.

Arnórsson, S., Guðmundsson, G., Sigurmundsson, S., G., Björnsson, A., Gunnlaugsson, E., Gíslason, G., Jónsson, J., Einarsson, P., Björnsson, S., 1975. Systematic exploration of the Krísuvík high-temperature area, Reykjanes-Peninsula, Iceland. Report, National Energy Authority, Reykjavik, Iceland. OS/JHD 7554, 127 pp.

Arnórsson, S., Stefánsson, A., Bjarnason, J.Ö., 2007. Fluid-fluid interactions in geothermal systems. Rev. Mineral. Geochem., 65, 259-312.

Barry, P.H., Hilton, D.R., Füri, E., Halldórsson, S.A., Grönvold, K., 2014. Carbon isotope and abundance systematics of Icelandic geothermal gases, fluids and subglacial basalts with implications for mantle plume-related CO_2 fluxes. Geochim. et Cosmochim. Acta, 134, 74-99.

Barth, T.F.W., 1950. Volcanic geology, hot springs and geysers of Iceland. Carnegie Inst. of Wash. Washington, D.C. pp. 174.

Bjarnason, J.O., 2000. A note on the chemical composition of geothermal steam from well KR-9 in Krýsuvík, southwestern Iceland. Report JÖB-2000/01, March, 2000.

Burton, M.R., Salerno, G.G., La Spina, A., Stefansson, A., Kaasalainen, H., 2010. Measurements of volcanic gas emissions during the first phase of 2010 eruptive activity of Eyjafallajokull, in: Presented at the AGU Fall Meeting, Abstract V41E-2310. AGU, San Francisco, California.

Burton, M., La Spina, A., Ilyinskaya, E., Salerno, G., 2014. Open path FTIR and SO2 camera measurements of the Holuhraun eruption Iceland 2014 in: Presented at the 12th Field Workshop on Volcanic Gases, CCVG, Atacama, Chile.

Chase, M.W., 1998. NISTJANAF Thermochemical Tables, 4th ed. J. Phys. Chem. Ref. Data Monograph, 9.

Chiodini, G., Marini, L., 1998. Hydrothermal gas equilibria: the H_2O–H_2–CO_2–CO–CH_4 system. Geochim. Cosmochim. Acta 62, 2673–2687.

D'Amore, F., Panichi C., 1980. Evaluation of deep temperature of hydrothermal systems by a new gas-geothermometer. Geochim. Cosmochim. Acta 44, 549–556.

Daveler, S.A., Wolery, T.J., 1992. EQPT, A Data File Preprocessor for the EQ3/6 Software Package: User's Guide and Related Documentation (Version 7.0). Report UCRL-MA-110662 PT II, Lawrence Livermore National Laboratory, Livermore, California.

Denbigh, K., 1971. The Principles of Chemical Equilibrium, 3rd ed. Cambridge University Press, Cambridge.

Di Napoli, R., Aiuppa, A., Allard, P., 2013. First multi-GAS based characterization of the Boiling Lake volcanic gas (Dominica, Lesser Antilles). Ann. Geophys. 56, 5, S0559; doi:10.4401/ag-6277.

Doukas, M. P., Gerlach, T. M., 1995. Sulfur dioxide scrubbing during the 1992 eruptions of Crater Peak, Mount Spurr Volcano, Alaska. U.S. Geol. Surv. Bull. B-2139, 47–57.

Flaathen, T., Gíslason, S.R., 2007. The effect of volcanic eruptions on the chemistry of surface waters: The 1991 and 2000 eruptions of Mt. Hekla, Iceland. JVGR, 164, 293-316.

Flaathen, T., Gíslason, S.R., Oelkers, E., Sveinbjornsdottir, A., 2009. Chemical evolution of the Mt. Hekla, Iceland, groundwaters: A natural analogue for CO_2 sequestration in basaltic rocks. Appl. Geochem., 24, 463-474.

Fournier, R.O., 1989. Geochemistry and dynamics of the Yellowstone National Park hydrothermal system. Annual Review of Earth and Planetary Sciences, 17, 13-53.

Garcia, S., Arnaud, N., Angelier, J., Bergerat, F., Homberg, C., 2003. Rift jump processes in Northern Iceland since 10 Ma from $^{40}Ar/^{39}Ar$ geochronology. Earth Planet. Sci. Lett. 214, 529–544.

Gerlach, T.M., McGee, K.A., Doukas, M.P., 2008. Emission rates of CO_2, SO_2, and H_2S, scrubbing, and pre-eruption excess volatiles at Mount St. Helens, 2004–2005, in Sherrod, D.R., Scott, W.E., Stauffer, P.H. (Eds.), A Volcano Rekindled: The Renewed Eruption of Mount St. Helens, 2004–2006. U.S. Geol. Surv. Prof. Pap. 1750, pp. 554–571.

Giggenbach, W.F., 1980. Geothermal gas equilibria. Geochim. Cosmochim. Acta 44, 2021–2032.

Giggenbach, W.F., 1981. Geothermal mineral equilibria. Geochim. Cosmochim. Acta 45, 393-410.

Giggenbach, W.F., 1984. Mass transfer in hydrothermal alterations systems. Geochim. Cosmochim. Acta 48, 2693–2711.

Giggenbach, W.F., 1987. Redox processes governing the chemistry of fumarolic gas discharges from White Island, New Zeland. Appl. Geochem. 2, 143–161.

Giggenbach, W.F., 1988. Geothermal solute equilibria. Derivation of Na-K-Mg-Ca geoindicators. Geochim. Cosmochim. Acta 52, 2749–2765.

Giggenbach, W.F., 1993. Redox control of gas compositions in Philippine volcanic-hydrothermal systems. Geothermics 22, 575–587.

Gíslason, S.R., Andrésdóttir, A., Sveinbjörnsdóttir, Á., Oskarsson, N., Thordarson, T., Torssander, P., Novâk, M., Zâk, K., 1992. Local effects of volcanoes on the hydrosphere: example from Hekla, southern Iceland. Water-rock Interaction: Rotterdam, Balkema 1, 477–481.

Gíslason, S.R., Oelkers, E.H., 2003. The mechanism, rates, and consequences of basaltic glass dissolution: II. An experimental study of the dissolution rates of basaltic glass as a function of pH at temperatures from 6°C to 150°C. Geochim. Cosmochim. Acta 67, 3817–3832.

Gíslason, S.R., Stefánsdóttir, G., Pfeffer, M.A., Barsotti, S., Jóhannsson, Th., Galeczka, I., Bali, E., Sigmarsson, O., Stefánsson, A., Keller, N.S., Sigurdsson, Á., Bergsson, B., Galle, B., Jacobo, V.C. Arellano, S., Aiuppa, A., Jónasdóttir, E.B., Eiríksdóttir, E.S., Jakobsson, S., Guðfinnsson, G.H., Halldórsson, S.A., Gunnarsson, H., Haddadi, B., Jónsdóttir, I., Thordarson1, M. Riishuus, Th., Högnadóttir, Th., Dürig, T., Pedersen, G.B.M., Höskuldsson, Á., Gudmundsson, M.T., 2015. Environmental pressure from the 2014–15 eruption of Bárðarbunga volcano, Iceland. Geochem. perspect. lett. doi: 10.7185/geochemlet.1509.

Guðjónsdóttir, S.R., 2014. Gas emissions from the Krýsuvík high-temperature geothermal system, Iceland. Master's thesis, Faculty of Earth Sciences, University of Iceland, 72 pp.

Guðmundsson, G., Arnórsson, S., Sigurmundsson, S, G., Björnsson, A., Gunnlaugsson, E., Gíslason, G., Jónsson, J., Einarsson, P., Björnsson, S., 1975. The Krýsuvík area, report on geothermal observations (in Icelandic). Report OSJHD 7554, November 1975, 71 pp.

Gysi, A.P., and Stefánsson, A., 2011. CO_2-water-basalt interaction. Numerical simulation of low temperature CO_2 sequestration into basalts. Geochim. Cosmochim. Acta 75, 4728-4751.

Gysi, A.P., and Stefánsson, A., 2012. Experiments and geochemical modeling of CO_2 sequestration during hydrothermal basalt alteration. Chemical Geology 306–307, 10–28.

Helgeson, H.C., 1968. Evaluation of irreversible reactions in geochemical processes involving minerals and aqueous solutions: I. Thermodynamic relations. Geochim. Cosmochim. Acta 32, 853–877.

Helgeson, H.C., Garrels, R.M., Mackenzie, F.T., 1969. Evaluation of irreversible reactions in geochemical processes involving minerals aqueous solutions: II. Applications. Geochim. Cosmochim. Acta 33, 455–481.

Henley, R.W., Truesdell, A.H., Barton, P.B.Jr, Whitney, J.A., 1984. Fluid-mineral equilibria in hydrothermal systems. Rev. Econ. Geol. 1.

Holm, N.G., Gíslason, S.R., Sturkell, E., Torssander, P., 2010. Hekla cold springs (Iceland): groundwater mixing with magmatic gases. Isot. Environ. Health Stud. 46, 180–189.

Höskuldsson, A., Hey, R., Kjartansson, E., Gudmundsson, G.B., 2007. The Reykjanes Ridge between 63°10′N and Iceland. J. Geodyn., 43, 73-86.

Kaasalainen, H., Stefánsson, A., 2012. The chemistry of trace elements in surface geothermal waters and steam, Iceland. Chem. Geol., 330-331, 60-85.

Kurz, M.D., Meyer, P.S., Sigurdsson, H.,1985. Helium isotope systematics within the neo-volcanic zones of Iceland. Earth Planet. Sci. Lett. 74, 29 l-305.

Ilyinskaya, E., Aiuppa, A., Bergsson, B., Di Napoli, R., Fridriksson, T., Óladóttir, A.A., Óskarsson, F., Grassa, F., Pfeffer, M., Lechner, K., 2015. Degassing regime of Hekla volcano 2012-2013. Geochim. Cosmochim. Acta. 159, 80–99.

Larsen, G., Dugmore, A., Newton, A., 1999. Geochemistry of historical-age silicic tephras in Iceland. The Holocene 9, 463-471.

Macpherson, C.G., Hilton, D.R, Day, J.M.D, Lowry, D., Grönvold, K., 2005. High $^3He/^4He$, depleted mantle and low-$\delta^{18}O$, recycled oceanic lithosphere in the source of central Iceland magmatism. Earth Planet. Sci. Lett. 223, 411-427.

Markússon, S., Stefánsson, A., 2011. Geothermal surface alteration of basalts, Krýsuvík Iceland-Aleteration mineralogy, water chemistry and the effects of acid supply on the alteration process. J.Volc. Geoth. Res. 206, 46-59.

Marini, L., Gambardella, B., 2005. Geochemical modeling of magmatic gas scrubbing. Ann. Geophys. 48, 739-753.

Marty B., Gunnlaugsson E., Jambon A., Oskarsson N., Ozima M., Pineau F. and Torssander P., 1991. Gas geochemistry of geothermal fluids, the Hengill area, southwest rift zone of Iceland. Chem. Geol. 91, 207-225.

Moune, S., Gauthier, P.J., Gíslason, S.R., Sigmarsson, O., 2006. Trace element degassing and enrichment in the eruptive plume of the 2000 eruption of Hekla volcano, Iceland. Geochim. Cosmochim. Acta 70, 461–479.

Moune, S., Sigmarsson, O., Thordarson, T., Gauthier, P.J., 2007. Recent volatile evolution in the magmatic system of Hekla volcano, Iceland. Earth Planet. Sci. Lett. 255, 373–389.

Nordstrom, K.D., McCleskey, B.R., Ball, J.W., 2009. Sulfur geochemistry of hydrothermal waters in Yellowstone National Park: IV Acid-sulfate waters. Appl. Geochem., 24, 191-207.

Oelkers, E.H., Gíslason, S.R., 2001. The mechanism, rates, and consequences of basaltic glass dissolution: I. An experimental study of the dissolution rates of basaltic glass as a function of aqueous Al, Si, and oxalic acid concentration at 25°C and pH=3 and 11. Geochim. Cosmochim. Acta 65, 3671-3681.

Oskarsson, N., 1984. Monitoring of fumarole discharge during the 1975-1982 rifting in Krafla volcanic center, north Iceland. J. Volc. Geoth. Res. 22, 97-121.

Peate, D. W., Baker, J. A., Jakobsson, S, P., Waight, T. E., Kent, A. J. R., Grassineau, N. V., Skovgaard, A. C., 2009. Historic magmatism on the Reykjanes Peninsula, Iceland: a snap shot of melt generation at a ridge segment. Contrib. Mineral. Petrol. 157, 359-382.

Pfeffer, M.A., Stefánsdóttir, G., Bergsson, B., Barsotti, S., Galle, B., Conde, V., Donovan, A., Aiuppa, A., Burton, M., Keller, N.S., Askew, R.A., Ilyinskaya, E., La Spina, A., Sigurðardóttir, G.M., Jónasdóttir, E.B., Snorrason, A., Stefánsson, A., Tsanev, V., 2015. Ground-based measurements of the emission rate and composition of gases from the Holuhraun eruption, in: Presented at the EGU Fall Meeting, Abstract 2015-7373, Vienna, Austria.

Polak, B.G., Kononovi, I., Tolstikhin, I.N., Mamyrin, B.A., Khabarin, L., 1976. The helium isotopes in thermal fluids, in: Thermal and Chemical Problems of Thermal Waters. Int. Assoc. Hydrol. Sci. 119, pp. 17-33.

Poreda, R.J., Schilling, J.G., Craig, H., 1980. $^{3}He/^{4}He$ variations along the Reykjanes Ridge. Eos 61, 1158.

Poreda, R.J., Schilling, J.G., Craig, H., 1986. Helium and hydrogen isotopes in ocean ridge basalts north and south of Iceland. Earth Planet. Sci. Lett. 78, 1-17.

Poreda R., Craig H., Arnórsson S., Welhan J., 1992. Helium isotopes in Icelandic geothermal systems: I. ^{3}He, gas chemistry, and ^{13}C relations. Geochim. Cosmochim. Acta 56, 4221–4228.

Reed, M.H., 1982. Calculation of multicomponent chemical equilibria and reaction processes in systems involving minerals, gases and an aqueous phase. Geochim. Cosmochim. Acta 46, 513-528.

Reed, M.H., 1997. Hydrothermal alteration and its relationship to ore fluid composition, in: Barnes, H.L. (Ed.), Geochemistry of Hydrothermal Ore Deposits, 3rd ed. Wiley, New York, pp. 303-366.

Reed, M.H., 1998. Calculation of simultaneous chemical equilibria in aqueous-mineral-gas systems and its application to modeling hydrothermal processes, in: Richards, J., Larson, P. (Eds.), Techniques in Hydrothemal Ore Deposits Geology. Rev. Econ. Geol. 10, 109-124.

Reed, M.H., Spycher, N.F. 1984. Calculation of pH and mineral equilibria in hydrothermal water with application to geothermometry and studies of boiling and dilution. Geochim. Cosmochim. Acta, 48, 1479-1490.

Sæmundsson, K., 1974. Fissure swarms and central volcanoes of the neovolcanic zones of Iceland. Geol. Soc. Am. Bull. 85, 495–504.

Sigvaldason, G.E., 1966. Chemistry of thermal waters and gases in Iceland. Bull. Volcanol. 29, 589-604.

Sigvaldason, G, E., Ellísson, G., 1968. Collection and analysis of volcanic gases at Surtsey, Iceland. Geochim.Cosmochimi. Acta 32, 797-805.

Shinohara, H., Yoshikawa, S., Miyabuchi, Y., 2015. Degassing Activity of a Volcanic Crater Lake: Volcanic Plume Measurements at the Yudamari Crater Lake, Aso Volcano, Japan, in: Rouwet, D., Christenson, B., Tassi, F., Vandemeulebrouck, J. (Eds.), Volcanic Lakes, ISBN: 978-3-642-36832-5 (Print) 978-3-642-36833-2 (Online).

Symonds, R.B., Reed, M.H., 1993. Calculation of multicomponent chemical equilibria in gas-solid-liquid systems: calculation methods, thermochemical data and applications to studies of high-temperature volcanic gases with examples from Mount St. Helens. Am. J. Sci. 293, 758-864.

Symonds, R.B., Gerlach, T.M., Reed, M.H., 2001. Magmatic gas scrubbing: implications for volcano monitoring. J. Volcanol. Geotherm. Res. 108, 303–341.

Symonds, R.B., Janik, C.J., Evans, W.C., Ritchie, B.E., Counce, D.A., Poreda, R.J., Iven, M., 2003. Scrubbing masks magmatic degassing during repose at Cascade-Range and Aleutian-Arc volcanoes. U.S. Geol. Surv. Open File Rep. 03-0435, 22 pp.

Spycher, N.A., Reed, M.H., 1988. Fugacity coefficients of H_2CO_2, CH_4, H_2O and H_2O-CO_2-CH_4 mixtures: a virial equation treatment for moderate pressures and temperatures applicable to calculations of hydrothermal boiling. Geochim. Cosmochim. Acta 52, 739-749.

Stefánsson, A., Arnórsson, S., 2000. Feldspar saturation state in natural waters. Geochim.Cosmochim. Acta, 64, 2567-2584.

Stefánsson, A., Arnórsson, S., 2002. Gas pressures and redox reactions in geothermal fluids in Iceland. Chem. Geol. 190, 251–271.

Tamburello, G., Hansteen, T., Bredemeyer, S., Aiuppa, A., Tassi, F., 2014. Gas emissions from five volcanoes in northern Chile and implications for the volatiles budget of the Central Volcanic Zone. Geophys. Res. Lett. 41, 4961–4969.

Thordarson, T., Larsen, G., 2007. Volcanism in Iceland in historical time: Volcano types, eruption styles and eruptive history. J. Geodynam. 43, 118–152.

Ward, P.L., Björnsson, S., 1971. Microearthquakes, swarms, and the geothermal areas of Iceland. J. Geophys. Res. 76, 3953-3982.

Werner, C., Hurst, T., Scott, B., Sherburn, S., Christenson, B.W., Britten, K., Cole-Baker, J., Mullan, B., 2008. Variability of passive gas emissions, seismicity, and deformation during crater lake growth at White Island Volcano, New Zealand, 2002–2006. J. Geophys. Res. 113, B01204, doi:10.1029/2007JB005094.

Werner, C., Evans, W., Kelly, P., McGimsey, R., Pfeffer, M., Doukas, M., Neal, C., 2012. Deep magmatic degassing versus scrubbing: Elevated CO_2 emissions and C/S in the lead-up to the 2009 eruption of Redoubt Volcano, Alaska. Geochem. Geophys. Geosyst. 13, 1-18, doi:10.1029/2011GC003794.

White, D.E., 1957. Thermal waters of volcanic origin. Geol. Soc. Am. Bull. 68, 1637-1658.

Wolery, T. J., 1979. Calculation of Chemical Equilibrium between Aqueous Solutions and Minerals: The EQ3/6 Software Package. Report UCRL-52658, Lawrence Livermore National Laboratory, Livermore, California.

Wolery, T.J., 1992a. EQ3/6, A Software Package for Geochemical Modeling of Aqueous Systems: Package Overview and Installation Guide (Version 7.0). Report UCRL-MA-110662 PT I, Lawrence Livermore National Laboratory, Livermore, California.

Wolery, T.J., 1992b. EQ3NR, A Computer Program for Geochemical Aqueous Speciation-Solubility Calculations: Theoretical Manual, User's Guide, and Related Documentation (Version 7.0). Report UCRL-MA-110662 PT III, Lawrence Livermore National Laboratory, Livermore, California.

Wolery, T.J., Daveler, S.A., 1992. EQ6, a computer program for reaction path modeling of aqueous geochemical systems: theoretical manual, user's guide and related documentation (version 7.0). Report UCRl-MA-110662 PT IV, Lawrence Livermore National Laboratory, Livermore, California.

Wolff-Boenisch, D., Gíslason, S.R., Oelkers, E.H., Putnis, C.V., 2004. The dissolution rates of natural glasses as a function of their composition at pH 4 and 10.6, and temperatures from 25 to 74°C. Geochim. Cosmochim. Acta 68, 4843–4858.

10. CAPTIONS

Figure 1: *(a)* Simplified geological map of Iceland (modified from Thordarson and Larsen, 2007), showing the location of the main volcanic and geothermal systems on which the gas dataset (Table 3) is based upon. RR, Reykjanes Ridge; RVB, Reykjanes Volcanic Belt; SISZ, South Iceland Seismic Zone; WVZ, West Volcanic Zone; MIB, Mid-Iceland Belt; EVZ, East Volcanic Zone; NVZ, North Volcanic Zone; TFZ, Tjörnes Fracture Zone; KR, Kolbeinsey Ridge; ÖVB, Öræfi Volcanic Belt; SVB, Snæfellsnes Volcanic Belt; *(b)* Triangular plot of $H_2O/10$-CO_2-$5S_{TOT}$ abundances in hydrothermal and magmatic gas samples from Iceland (for data source, see Table 3). S_{TOT} is total sulfur (e.g., H_2S + SO_2). Magmatic, hydrothermal and cold gas samples plot into compositionally distinct domains (see Text for discussion).

Figure 2: Sequence of computational operations to model magmatic scrubbing: combination of reaction path models (EQ3/6 model runs) with degassing calculations. Each *model run* listed in Table 2 is composed of a sequence of EQ3/6 runs; in each, n_{g,run_1} moles of *initial gas* and n_s moles of *solid reactant* are added to a *starting aqueous solution* to initiate the model reaction path. Temperature (T_{run}) and pressure (P_{run}) conditions of each run are fixed a-priori (see Section 4 and Appendix A). The new model solution (*solution_1*), obtained at the end of the reaction path, (if in a state of over-pressure: $Pgas_{TOT} > P_{run}$), is degassed (single-step degassing calculation routine; cfr. Section 2.3), until attainment of equilibrium ($Pgas_{TOT} = P_{run}$), thus obtaining the chemical compositions of *degassed aqueous solution* and *separated gas phass*. The resulting *degassed aqueous solution* is used as *starting aqueous solution* in the next run. This sequence of EQ3/6 run simulations and degassing calculations are iteratively repeated (see Appendix A).

Figure 3: *(a)* Model evolution of pH in the 8 different model runs (Table 2). In low-T model run (A-D, Table 2), the pH of model solutions decreases as increasing amounts of *initial gas* are added. The aqueous solutions modelled by high-T model runs (E-H; Table 2) are characterized by neutral to basic pH values, due to more effective dissolution of *solid reactant*, in the 200-250°C temperature range. The pHs of high-T model *aqueous solutions* agree well with measured pH values of Krýsuvík reservoir waters (orange squares). Acidic steam-heated waters from the Krýsuvík geothermal system (sky blue squares) are best reproduced by a low temperature (< 100 °C) steam-heating process, here illustrated by a yellow-coloured model line. This model trend was numerically simulated in EQ3/6 by stepwise adding increasing amounts (from 5 to 10 moles) of a Krýsuvík hydrothermal steam into the *initial aqueous solution* (blue square) (cfr. Section 6.2.3); *(b)* Model evolution of redox conditions (as expressed by the logarithm of the oxygen fugacity, Log f_{O2}, in bar). Reducing redox conditions (Log f_{O2} ~ -70) are produced in the low-T runs in response to the first addition of *initial gas* to the *initial aqueous solution* (Log f_{O2} = -0.6). Afterwards, the Log f_{O2}

of model *aqueous solutions* progressively increases with temperature, up to Log f_{O2} ~ -47 at 106°C. In high-T model runs, oxygen fugacity was externally fixed by the empirical relation of D'Amore and Panichi (1980). Data sources in Figures *(a)*: Arnórsson et al., 1975 [1]; Flaatheen and Gíslason, 2007 [2]; Holm et al., 2010 [3]; Markússon and Stefánsson, 2011 [4]; Guðmundsson et al., 1975 [5].

Figure 4: Model evolution of major anion *(a)* and cation *(b)* species in the different model runs (Table 2). In low-T model runs, model *aqueous solutions* evolve, through the reaction path, from the carbon- magnesium-rich composition of the *initial aqueous solution* (blue square) towards compositions enriched in sulphur and, to a minor extent, chlorine (as Cl^-), reflecting magmatic gas addition. No evident change is observed for dissolved cations (low-T model *aqueous solutions* all cluster on the Mg-corner). High-T model runs yield Na-K-Cl-rich aqueous solutions that match well the compositions of the hottest hydrothermal reservoir waters sampled by boreholes at Krýsuvík (orange squares). Mixing lines between modelled Na-K-Cl solutions and cold waters (represented by *initial aqueous solution* – blue square) are illustrated by dashed lines. The acidic shallow waters of Krýsuvík are well reproduced by our steam-heating model line (see caption of Figure 3).

Figure 5: Scatter plot of total gas pressure ($Pgas_{TOT}$) of model *aqueous solutions* vs. the amount of *initial gas* added in the runs. Run pressure (P_{run}; Figure 2) is fixed at 1.013bar in low-T model runs and as the water saturation pressure at run temperature (15.537 bar at 200°C and 39.736 bar at 250°C) in high-T model runs (see also Appendix A). As a consequence of the addition of *initial gas* to the *starting aqueous solution*, total pressure of dissolved gases ($Pgas_{TOT} = P_{H_2O} + P_{CO_2} + P_{H_2S} + \ldots$) in the model *aqueous solutions* increase, and over-saturation is eventually reached when $Pgas_{TOT}$ exceeds P_{run}. Saturation is achieved at ~0.6mols of gas added in low-T runs; similarly, over-pressured solutions are obtained by addition of >0.2 moles (200°C) or >0.8 moles (at 250°C).

Figure 6: Temperature-dependent model evolution of the composition of model gases. Upon increasing temperatures, the model *separated gas* phase changes from CO_2-dominated (for temperatures ≤80°C) to H_2O-dominated (temperatures in the 80-250°C range). In low-temperature runs, *separated gas* are depleted (by gas scrubbing) in sulphur (as $H_2S_{(g)}$) and chlorine (as $HCl_{(g)}$), relative to the composition of the *initial gas*. For the high-T runs, the plot illustrates the compositions of both (i) *dissolved gases* in model aqueous solutions (*model reservoir waters*), and (ii) the free gas phase (*separated gas*) released from high-T model solutions (the free gas is formed

by single-step separation of model solutions when the gas overpressure threshold is reached; see Section 2.3). Sulfur gas-phase transport is enhanced at 200-250°C, while $HCl_{(g)}$ preferentially partitions into *aqueous solutions* even in such extreme conditions.

Figure 7: Modeled vs. natural gas compositions at match. Volcanic gas CO_2/S_{TOT} ratios (mean - μ; Table 3) in surface gas discharges and borehole fluids from Icelandic volcano/hydrothermal systems, plotted against temperature. For cold gas samples (Hk and Gr; Table 3) and hydrothermal steam vents (fumaroles; squares in Figure), the surface discharge temperatures are used. The steam samples (WS, crosses in Figure) and deep reservoir water (WW, stars in Figure), collected in boreholes, are plotted at their sampling temperatures (200-340°C). For reservoir waters, the CO_2/S_{TOT} ratios refer to the *dissolved gas* phase. The CO_2/S_{TOT} ratios of the model gases (calculated from the results in Figure 6) are shown for comparison, demonstrating reasonable agreement with observed gas compositions (model curve identification codes are from Table 2). Low-T run model *separated gases* correspond to the compositions of Icelandic cold gas samples; while high-T model runs output model gas compositions that reproduce well the CO_2/S_{TOT} ratio range of Icelandic hydrothermal reservoir fluids (steam and *dissolved gas* in reservoir waters). Gas ratios in surface fumaroles are matched by compositions of gases formed by boiling at 100°C of high-T (200-250°C) model aqueous solutions.

Figure 8: Modeled vs. natural gas compositions at match. Scatter plot of volcanic gas CO_2/S_{TOT} ratios vs. H_2O/CO_2 ratios in surface gas discharges and borehole fluids from Icelandic volcano/hydrothermal systems. The model-derived compositions of gas phases (calculated from model results in Figure 6) are shown for comparison, and demonstrate good agreement with observed gas compositions. *(a)* Model curves obtained in low-T run model runs (Table 2) demonstrate H_2O-poor, CO_2-rich compositions matching those of Icelandic cold gas samples. *(b)* High-T model runs (Table 2) output model aqueous solutions (model curves shown; see legend) that reproduce the *dissolved gas* phase composition of Icelandic reservoir waters, collected in deep boreholes; in the same panel, the composition of the equilibrium free gas phase separated from high-T model solutions (*separated gas*) is also indicated (see Text) *(c)* Model compositions of gases formed by boiling of 200-250°C model aqueous solutions, down to 100°C; these model gases overlap the compositional range of Icelandic hydrothermal steam samples (shown in (a)), and fit well the compositions of fumarolic steam discharges at Krýsuvík.

Figure A.1: Model run temperature (T_{run}) vs. amount of *initial gas* (mol) added per run. In low-T model runs, the temperature of each single run (T_{run_n}) (see also Figure 2) is calculated by enthalpy balance, according to Equation A.3. T_{run} increases proportionally to the moles of *initial* (magmatic) *gas* added to the *starting aqueous solution* (Table 2). Results for each run (e.g., A_1, A_2…; Table 2) and model run types (A-D; Table 2) are plotted (see legend), and describe four overlapping model trends. 6.6 moles of *initial gas* are required to raise the model run temperature (T_{run}), from 4.1°C (the temperature of the *initial aqueous solution*; blue square) to 106°C.

Table 1: Chemical composition of the aqueous solution and reactants (gas and solids) used to initialized the reaction path modeling here presented.

AQUEOUS SOLUTION			**GAS REACTANT**		**SOLID REACTANTS**			
sample RB1E[(2)]			**Fimmvörduháls fissural eruption from Eyjafjallajökull volcano**[(1)]		**basaltic andesitic glass**[(3)]		**basaltic glass**[(3)]	
initial aqueous solution			***initial gas***		***Hyd-Hekla-glass (solid reactants)***		***Hyd-Krýsuvík-glass (solid reactants)***	
T_w	4.1	°C	T_g	800°C	$SiAl_{0.31}O_2(OH)_{0.93}$		$SiAl_{0.32}O_2(OH)_{0.96}$	
Eh	0.8	Volt	H_2O	81.49 % in vol.				
pH	7.7		CO_2	15.28 % in vol.	***Hekla-glass-cations (special reactant)***[(*)]		***Hyd-Krýsuvík-glass (special reactant)***[(*)]	
SiO_2	21.71	mg/l	SO_2	3.06 % in vol.	Fe	0.174 mol	Fe	0.240 mol
Na^+	42.14	mg/l	HCl	0.18 % in vol.	Mg	0.076 mol	Mg	0.170 mol
Ca^{2+}	18.99	mg/l			Ca	0.130 mol	Ca	0.220 mol
K^+	2	mg/l			Na	0.142 mol	Na	0.090 mol
Mg^{2+}	17.395	mg/l			K	0.030 mol	K	0.008 mol
HCO_3^-	$3.20 \cdot 10^{-3}$	mol/kg			O	0.029 mol	O	0.223 mol
Cl^-	9.75	mg/l						
NO_3^- (as NH_3aq)	$3.22 \cdot 10^{-6}$	mol/kg						
SO_4^{2-}	22.8	mg/l						
Al^{3+}	0.016	mg/l						
Fe^{2+}	0.015	mg/l						

[(1)] Burton et al. (2010); [(2)] Holm et al. (2010); [(3)] Wolff-Boenisch et al. (2004); [(*)] *special reactant* chemical composition (see Appendix A for details)

Table 2: The 8 model run types. For each type, the table lists the number of runs performed, the run temperature range (T_{run}), the run pressure (P_{run}) and the *solid reactants* used. The amount of *initial gas* added in each run ($n_{g,run}$) and the *initial gas* relative dissolution rate are also indicated. Note that of the large amounts (n_s) of *solid reactants* available to dissolve in each model run type (from 77.26 mol to 289.23 mol), only a small fraction is actually consumed in the runs (listed in the column "consumed"). See Text and Appendix A

model run ID	**number of runs**	**model run T_{run} (°C)**	**model run P_{run} (bar)**	***initial gas*** **($n_{g,TOT}$; mol)**	***initial gas*** **added per run ($n_{g,run}$; mol)**	***initial gas*** **relative dissolution rate(*)**	***solid reactant*** **type**	***solid reactant*** **(n_s; mol)**	***solid reactant*** **"consumed" at each run (mol)**
LOW TEMPERATURE MODEL RUNS									
A_1-11	11	14-106	1.013	6.6	0.6	1	none	none	none
B_1-5	5	14-106	1.013	6.6	(0.6 at the first run) 1.5	25.45	*Hyd_Hekla_Glass*(1) *Hekla-glass-cations*(1)	77.26 77.26	0.022-0.059 0.022-0.059
C_1-5	5	14-106	1.013	6.6	(0.6 at the first run) 1.5	25.50	*Hyd_Hekla_Glass*(1) *Hekla-glass-cations*(1)	77.26 77.26	0.022-0.059 0.022-0.059
D_1-5	5	14-106	1.013	6.6	(0.6 at the first run) 1.5	26.00	*Hyd_Hekla_Glass*(1) *Hekla-glass-cations*(1)	77.26 77.26	0.022-0.059 0.022-0.059
HIGH TEMPERATURE MODEL RUNS									
E_1-7	7	200	15.537	2	(0.1 at the first run) 0.3	17	*Hyd_Krýsuvík_Glass*(1) *Krýsuvík-glass-cations*(1)	289.23 289.23	0.19-2.85 0.19-2.85
F_1-7	7	200	15.537	2	(0.1 at the first run) 0.3	100	*Hyd_Krýsuvík_Glass*(1) *Krýsuvík-glass-cations*(1)	289.23 289.23	0.19-2.85 0.19-2.85
G_1-7	7	250	39.737	2	(0.1 at the first run) 0.3	17	*Hyd_Krýsuvík_Glass*(1) *Krýsuvík-glass-cations*(1)	289.23 289.23	0.17-0.35 0.17-0.35
H_1-7	7	250	39.737	2	(0.1 at the first run) 0.3	100	*Hyd_Krýsuvík_Glass*(1) *Krýsuvík-glass-cations*(1)	289.23 289.23	0.17-0.35 0.17-0.35

(1) Wolff-Boenisch et al. (2004); (*)normalised to the solid reactant reaction rate (see Text and Appendix A for detail)

Table 3: Chemical composition of Icelandic gas samples (expressed as % in vol.), along with gas CO_2/S_{TOT} and H_2O/CO_2 (molar) ratios. For each volcanic-hydrothermal system, the mean (μ) and deviation standard (1σ) of each parameter are reported. Discharge gas temperatures (T_s; °C) and/or estimated equilibrium temperatures (T_{eq}; °C) are also listed for each gas manifestation. Natural gas samples include fumaroles, fumarolic plumes, and eruptive plumes. Geothermal borehole data include well steam (WS) samples and dissolved gases in reservoir waters (well waters: WW). Sampling techniques are also listed, and include direct sampling of the fumaroles, well steam and well water, and in-situ (Multi-GAS) or remote (FTIR) sensing of the near-vent plumes.

Site	Abbreviation and References	Type	Measurement technique	H_2O μ±1σ	CO_2 μ±1σ	H_2S μ±1σ	SO_2 μ±1σ	HCl μ±1σ	CO_2/S_{TOT} μ±1σ	H_2O/CO_2 μ±1σ	T_s	T_{eq} min-max
Askja	As [5], [7]	fumarole	direct sampling	98.9±1	0.9±0.1	$3.7\cdot10^{-2}\pm3\cdot10^{-2}$			22.8±8	235±127	95	
Bjarnarflag	Bj [5]	fumarole	direct sampling	99.1±0.6	0.4±0.2	$2.1\cdot10^{-1}\pm6\cdot10^{-2}$			1.9±1	348±248	95	
Eldfell	El [18]	fumarolic plume	MultiGAS	79.4±11.9	20.6±11.9	$1.3\cdot10^{-2}\pm1.1\cdot10^{-2}$			2603±1977	5.5±3.8	257	270
Eyjafjallajökull / Fimmvörduháls	Fi [12]	plume	FTIR	81.5	15.3		3.06	0.17	5	5.3	1125	
Fremrinamur	Fr [5]	fumarole	direct sampling	92.9	1	$3.3\cdot10^{-1}$			2.9	97.5	95	
Geysir	Ge [7]	fumarole	direct sampling	99.6	0.2	$7.6\cdot10^{-4}$			209	627	95	
Grimsfjall	Gr [18]	fumarolic plume	MultiGAS	83.9±26.4	16.1±26.4	$6.1\cdot10^{-3}\pm2.2\cdot10^{-3}$			5197±6812	11.6±43.4	94	
Hekla	Hk [16]	fumarolic plume	MultiGAS	35.6	64.4±27.8	$8.2\cdot10^{-3}\pm1.7\cdot10^{-2}$			61451±78690	1.23±1.4	33.2	
Hengill_WS	He_WS [7]	well steam	direct sampling	99.9	0.05	$2.8\cdot10^{-2}\pm2.7\cdot10^{-2}$			4.2±3	8345±7171	253	215-290
Hengill	He [7]	fumarole	direct sampling	99.1	0.7	$9.1\cdot10^{-2}$			7.6	143	95	
Holuhraun	Ho [14], [15], [17]	plume	FTIR - MultiGAS	96±2.2	2.1±1.3	1.9±1	0.03		1.13±0.49	75.8±53.7	1125	
Hveragerdi_WW	Hg_WW [6]	well waters	direct sampling	100	0.01	$8.2\cdot10^{-4}\pm4\cdot10^{-4}$			6.1±1	27770±15452	201	182-230
Hveragerdi_WS	Hg_WS [6], [9]	well steam	direct sampling	99.9	0.06	$7.1\cdot10^{-3}\pm1.8\cdot10^{-3}$			8.9±5	2140±1003	204	182-230
Hveragerdi	Hg [6]	fumarole	direct sampling	99.8±0.1	0.19±0.1	$7.6\cdot10^{-3}\pm4\cdot10^{-3}$			34.4±30	600±222	95	182-230

Hveravellir	Hv [5], [6]	fumarole	direct sampling	99.3±0.9	0.11	$9.6\cdot10^{-2}\pm1.1\cdot10^{-1}$			18.3±13	950±250	95	
Kerlingarfjöll	Ke [5], [7]	fumarole	direct sampling	99.4±0.1	0.38±0.1	$6.6\cdot10^{-2}\pm3\cdot10^{-2}$			6.8±3	274±56	95	
Köldukvíslarbotnar	Ko [7]	fumarole	direct sampling	99.5	0.4	$1.8\cdot10^{-2}$			23.8	235	95	
Krafla_WW	Kf_WW [4], [6], [7], [9]	well waters	direct sampling	99.2±1	0.7±0.8	$2.1\cdot10^{-2}\pm2.3\cdot10^{-2}$			48.2±52	2143±6541	288	190-340
Krafla_WS	Kf_WS [4], [6], [9]	well steam	direct sampling	99.1±1	0.8±0.9	$2.3\cdot10^{-2}\pm2.8\cdot10^{-2}$			47.9±46	1179±2546	326	190-340
Krafla	Kf [5], [6]	fumarole	direct sampling	91.9±6.8	6±5.2	$1.4\cdot10^{-1}\pm1\cdot10^{-1}$			58.9±42	29±26	95	
Krýsuvík_WW	Kr_WW [2], [3], [9]	well waters	direct sampling	100	3·10-3	$1.9\cdot10^{-4}$			65.1±80	38084±7505	157	267
Krýsuvík_WS	Kr_WS [11]	well steam	direct sampling	99.7	0.2	$1.9\cdot10^{-4}\pm1.9\cdot10^{-4}$			2.1	421		
Krýsuvík	Kr [6], [7], [8], [13]	fumarole	direct sampling - MultiGAS	99.2±0.7	0.7±0.6	$6.5\cdot10^{-2}\pm7\cdot10^{-2}$			17.3±17	224±97	95	
Kverkfjöll	Kv [5], [7]	fumarole	direct sampling	99.2±0.3	0.5±0.1	$4.5\cdot10^{-2}\pm1\cdot10^{-2}$			10.8±2	222±55	95	
Landmannalaugar	La [6]	fumarole	direct sampling	99.6±0.5	0.3±0.5	$2.2\cdot10^{-2}\pm2.8\cdot10^{-2}$			15.7±7	628±343	95	
Námafjall_WW	Na_WW [6]	well waters	direct sampling	99.9	0.05	$3.5\cdot10^{-2}\pm1.9\cdot10^{-2}$			1.5	2617±1315	283	246-320
Námafjall_WS	Na_WS [6], [7]	well steam	direct sampling	99.8	0.08	$7.6\cdot10^{-2}\pm2.6\cdot10^{-2}$			1.2	1428±566	302	246-320
Námafjall	Na [6], [7]	fumarole	direct sampling	99.8±0.1	0.13±0.04	$3.5\cdot10^{-2}\pm3\cdot10^{-2}$			8±11	810±220	95	
Nesjavellir_WW	Ne_WW [6]	well waters	direct sampling	99.9	0.1	$3.7\cdot10^{-2}\pm1.9\cdot10^{-2}$			4.4±3	972±188	281	271-290
Nesjavellir_WS	Ne_WS [6]	well steam	direct sampling	99.7	0.2±0.1	$9.4\cdot10^{-2}\pm3.8\cdot10^{-2}$			3.4±3	490±204	284	271-290
Nesjavellir	Ne [6]	fumarole	direct sampling	99.5±0.1	0.4	$6.7\cdot10^{-2}\pm2\cdot10^{-2}$			6.5±1	241±19	95	
Reykjanes_WW	Re_WW [6]	well waters	direct sampling	100	0.02	$9\cdot10^{-4}$			21.9	5066	248	248-285

Reykjanes_WS	Re_WS [6], [7], [9]	well steam	direct sampling	98.9	0.09	$3.6\cdot10^{-3}\pm4.5\cdot10^{-4}$			24.2±1	1175±201	267	248-285
Reykjanes	Re [5], [6], [7]	fumarole	direct sampling	98.2±2.8	1.7±2.7	$5.6\cdot10^{-2}\pm1\cdot10^{-1}$			66.8±47	299±225	95	
Surtsey	Su [1]	fumarole	direct sampling	87.8±4	4.1±3	$4.1\cdot10^{-1}\pm2.8\cdot10^{-1}$	3.03±0.62		1.2±0.8	52.6±58	1125	
Svartsengi_WW	Sv_WW [6]	well waters	direct sampling	100	0.02	$3.8\cdot10^{-4}\pm1.7\cdot10^{-4}$			45.6±11	6654±1029	240	240
Svartsengi_WS	Sv_WS[6], [7], [9]	well steam	direct sampling	99.9	0.08	$1.8\cdot10^{-3}\pm1.2\cdot10^{-3}$			51.8±17	1861±1264	240	240
Theistareykir	Th [5], [7]	fumarole	direct sampling	99.4±0.1	0.3±0.1	$7.6\cdot10^{-2}\pm3\cdot10^{-2}$			4.1±1	386±117	95	
Torfajökull	To [5], [7]	fumarole	direct sampling	99.6±0.3	0.3±0.2	$2.6\cdot10^{-2}\pm3.0\cdot10^{-2}$			20±10	408±204	95	
Vonarskard	Vo [5]	fumarole	direct sampling	99.1	0.4	0.1			3.5	274	95	

[1] Sigvaldson and Ellíson (1968); [2] Arnórsson, et al., 1975; [3] Guðmundsson et al. (1975); [4] Ármannsson et al. (1982); [5] Oskarsson (1984); [6] Arnórsson and Gunnlaugsson (1985); [7] Arnórsson (1986); [8] Arnórsson (1987); [9] Poreda et al. (1992); [10] Arnórsson (1995); [11] Bjarnason (2000); [12] Burton et al. (2010); [13] Guðjónsdóttir (2014); [14] Burton et al. (2014); [15] Gíslason et al. (2015); [16] Ilyinskaya et al. (2015); [17] Pfeffer et al. (2015); [18] This Study.

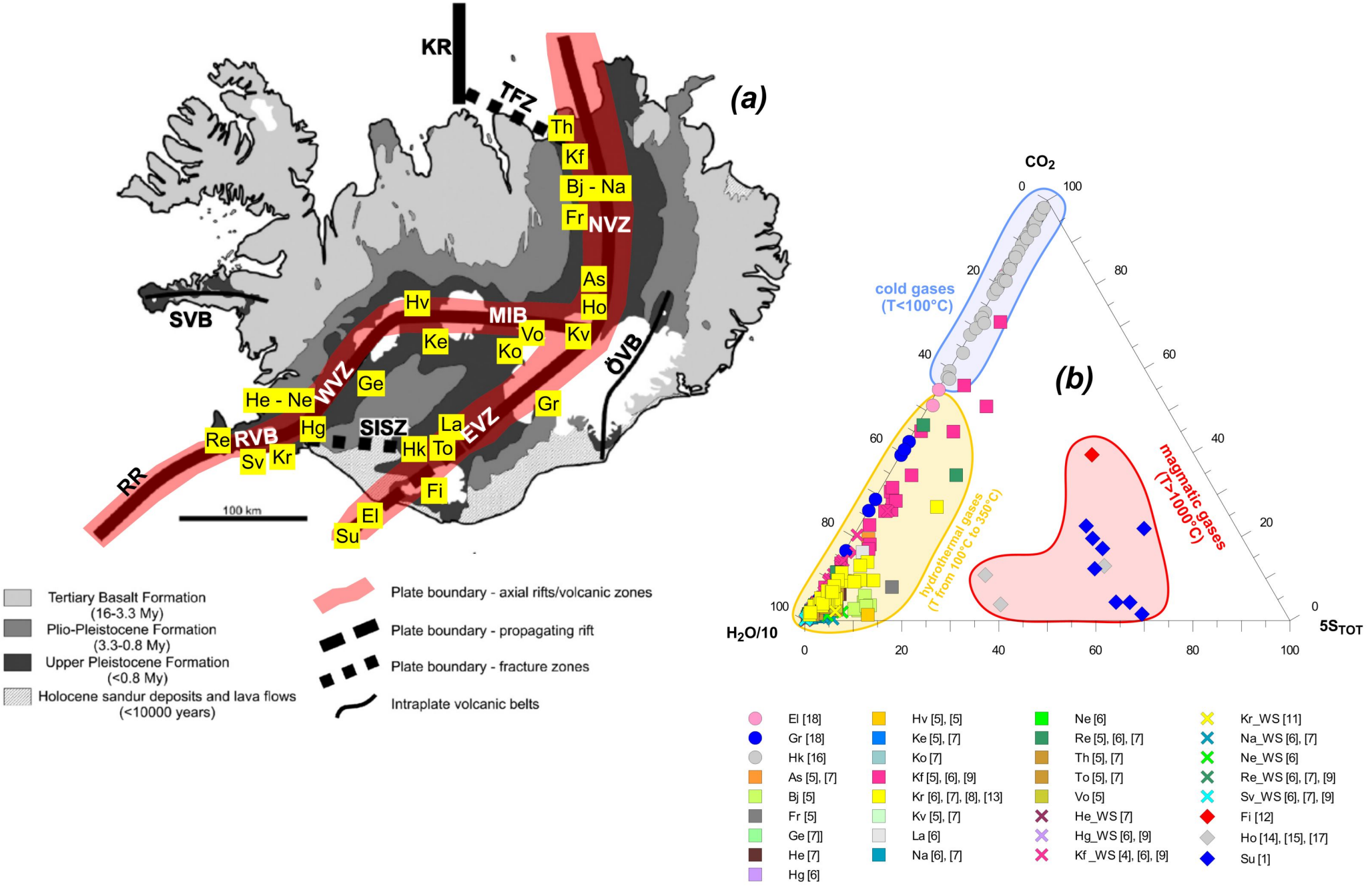
(a)
KR
TFZ
Th
Kf
Bj - Na
Fr
NVZ
As
Ho
Kv
Vo
MIB
Hv
Ke
Ko
SVB
ÖVB
WVZ
Ge
He - Ne
Gr
La
EVZ
Hg
SISZ
Re
RVB
Hk
To
Sv
Kr
RR
Fi
El
Su
100 km
Tertiary Basalt Formation (16-3.3 My)
Plio-Pleistocene Formation (3.3-0.8 My)
Upper Pleistocene Formation (<0.8 My)
Holocene sandur deposits and lava flows (<10000 years)
Plate boundary - axial rifts/volcanic zones
Plate boundary - propagating rift
Plate boundary - fracture zones
Intraplate volcanic belts
(b)
CO2
H2O/10
5STOT
cold gases (T<100°C)
hydrothermal gases (T from 100°C to 350°C)
magmatic gases (T>1000°C)
El [18]
Gr [18]
Hk [16]
As [5], [7]
Bj [5]
Fr [5]
Ge [7]]
He [7]
Hg [6]
Hv [5], [5]
Ke [5], [7]
Ko [7]
Kf [5], [6], [9]
Kr [6], [7], [8], [13]
Kv [5], [7]
La [6]
Na [6], [7]
Ne [6]
Re [5], [6], [7]
Th [5], [7]
To [5], [7]
Vo [5]
He_WS [7]
Hg_WS [6], [9]
Kf _WS [4], [6], [9]
Kr_WS [11]
Na_WS [6], [7]
Ne_WS [6]
Re_WS [6], [7], [9]
Sv_WS [6], [7], [9]
Fi [12]
Ho [14], [15], [17]
Su [1]

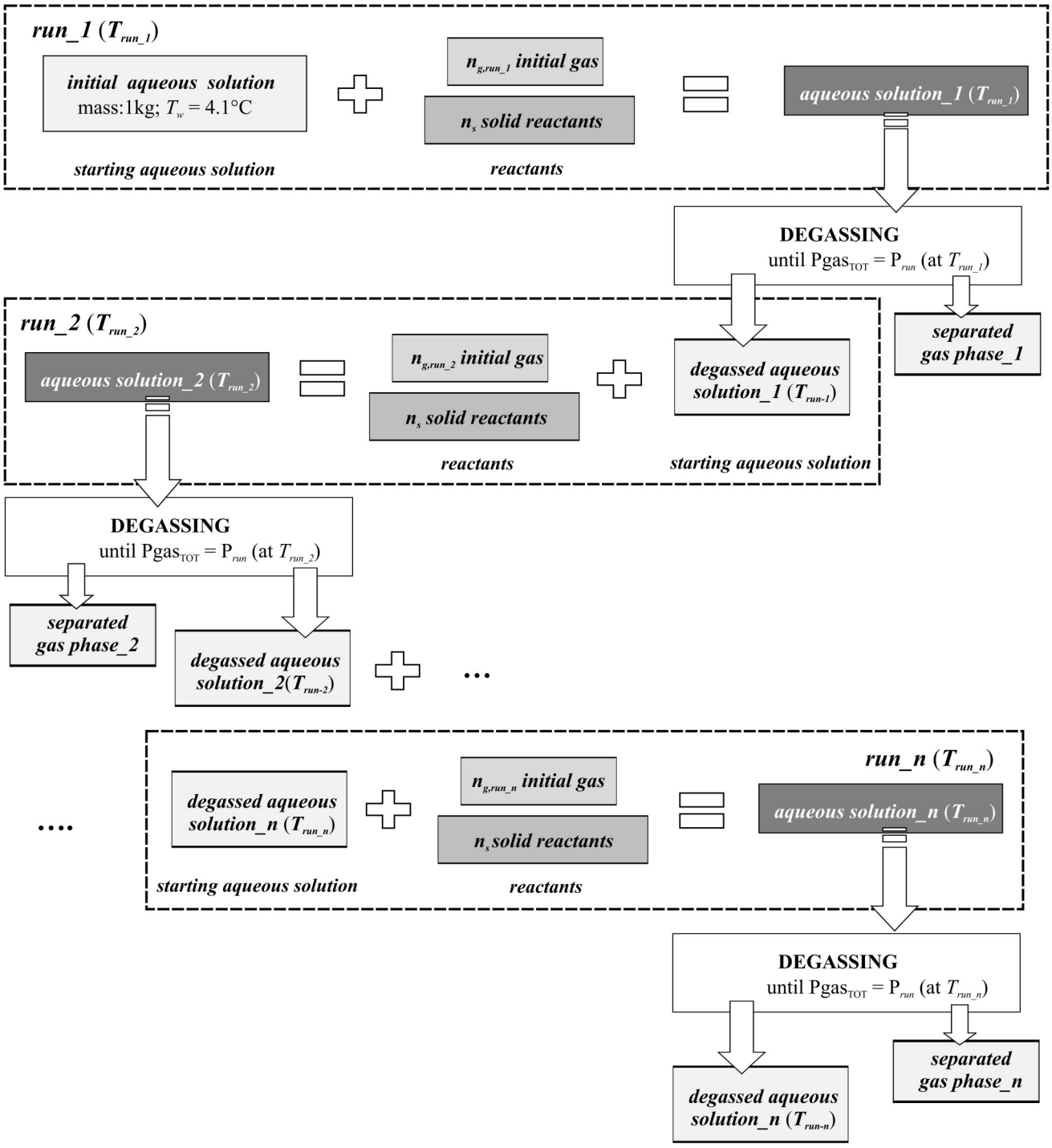
run_1 (T_{run_1})
initial aqueous solution
mass:1kg; T_w = 4.1°C
starting aqueous solution
n_{g,run_1} initial gas
n_s solid reactants
reactants
aqueous solution_1 (T_{run_1})
DEGASSING
until $Pgas_{TOT} = P_{run}$ (at T_{run_1})
separated gas phase_1
run_2 (T_{run_2})
aqueous solution_2 (T_{run_2})
n_{g,run_2} initial gas
n_s solid reactants
reactants
degassed aqueous solution_1 (T_{run-1})
starting aqueous solution
DEGASSING
until $Pgas_{TOT} = P_{run}$ (at T_{run_2})
separated gas phase_2
degassed aqueous solution_2(T_{run-2})
....
....
degassed aqueous solution_n (T_{run_n})
starting aqueous solution
n_{g,run_n} initial gas
n_s solid reactants
reactants
run_n (T_{run_n})
aqueous solution_n (T_{run_n})
DEGASSING
until $Pgas_{TOT} = P_{run}$ (at T_{run_n})
separated gas phase_n
degassed aqueous solution_n (T_{run-n})

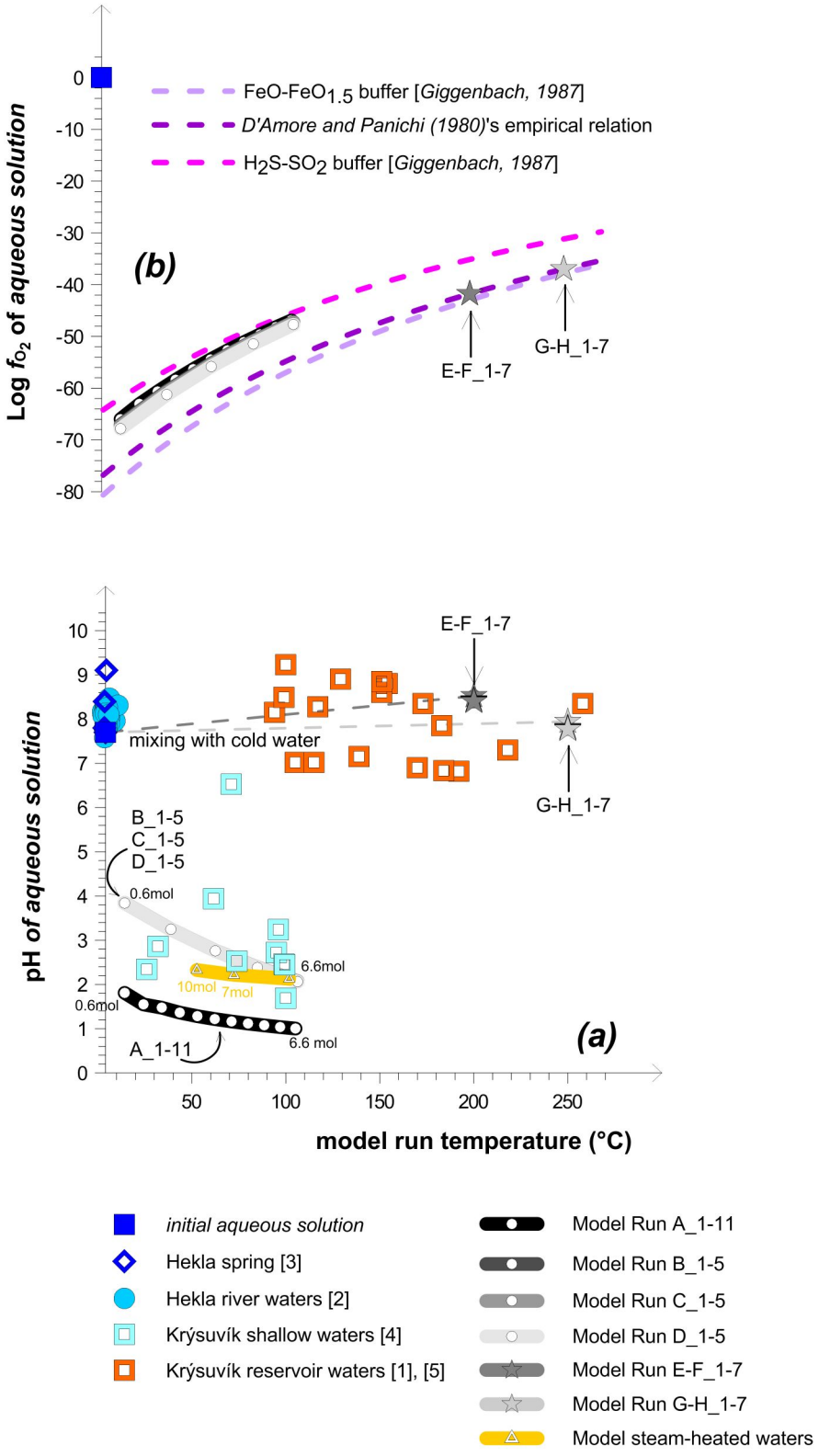
Log f_{O_2} of aqueous solution
0
-10
-20
-30
-40
-50
-60
-70
-80
FeO-FeO1.5 buffer [Giggenbach, 1987]
D'Amore and Panichi (1980)'s empirical relation
H2S-SO2 buffer [Giggenbach, 1987]
(b)
E-F_1-7
G-H_1-7
pH of aqueous solution
10
9
8
7
6
5
4
3
2
1
0
mixing with cold water
E-F_1-7
G-H_1-7
B_1-5
C_1-5
D_1-5
0.6mol
6.6mol
10mol
7mol
0.6mol
A_1-11
6.6 mol
(a)
50
100
150
200
250
model run temperature (°C)
initial aqueous solution
Hekla spring [3]
Hekla river waters [2]
Krýsuvík shallow waters [4]
Krýsuvík reservoir waters [1], [5]
Model Run A_1-11
Model Run B_1-5
Model Run C_1-5
Model Run D_1-5
Model Run E-F_1-7
Model Run G-H_1-7
Model steam-heated waters

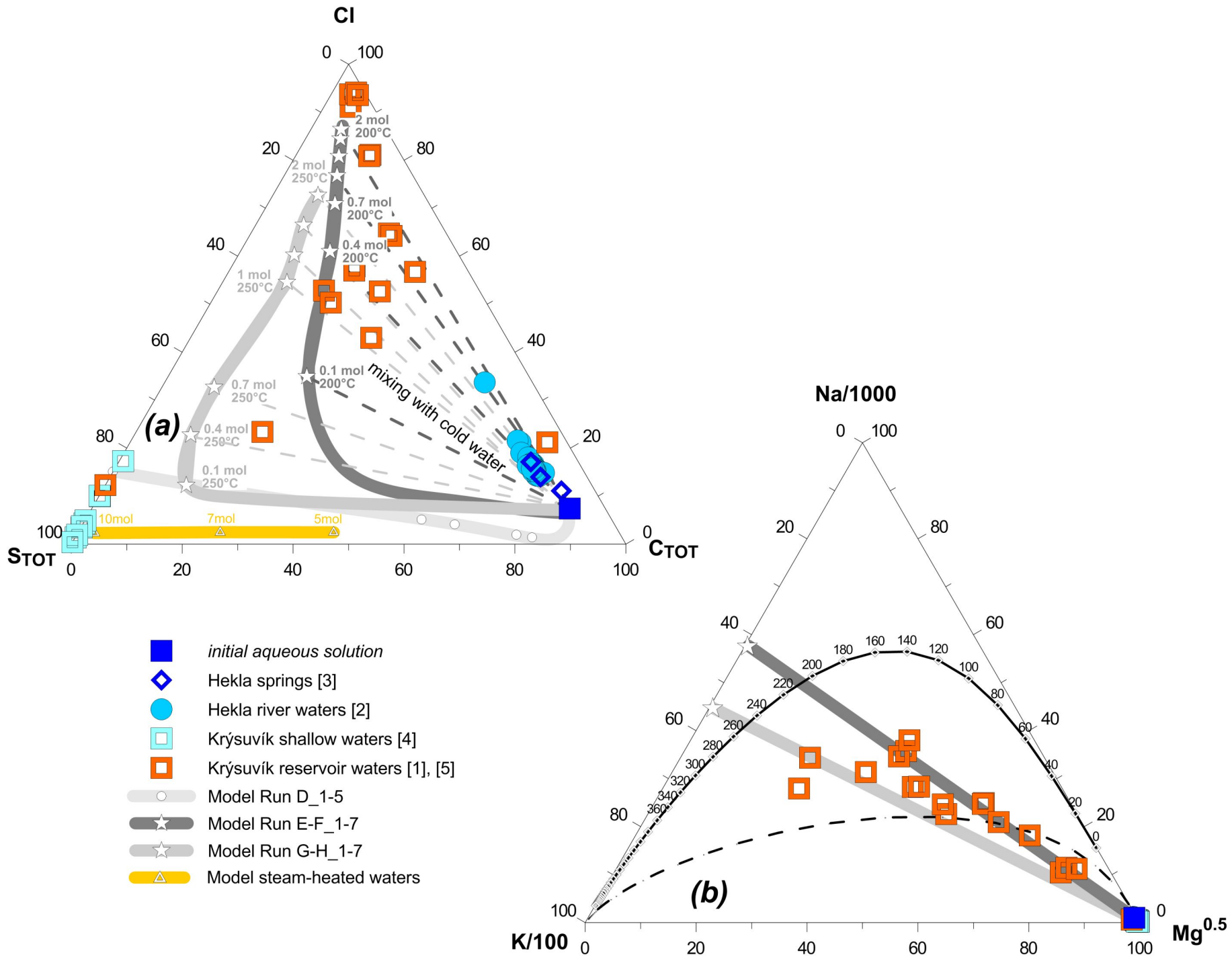
Cl
0
100
20
80
40
60
60
40
80
20
100
0
STOT
CTOT
0
20
40
60
80
100
2 mol 200°C
2 mol 250°C
0.7 mol 200°C
0.4 mol 200°C
1 mol 250°C
0.1 mol 200°C
mixing with cold water
0.7 mol 250°C
0.4 mol 250°C
0.1 mol 250°C
10mol
7mol
5mol
(a)
initial aqueous solution
Hekla springs [3]
Hekla river waters [2]
Krýsuvík shallow waters [4]
Krýsuvík reservoir waters [1], [5]
Model Run D_1-5
Model Run E-F_1-7
Model Run G-H_1-7
Model steam-heated waters
Na/1000
0
100
20
80
40
60
60
40
80
20
100
0
K/100
Mg0.5
0
20
40
60
80
100
180
160
140
120
100
200
220
240
260
280
300
320
340
360
(b)

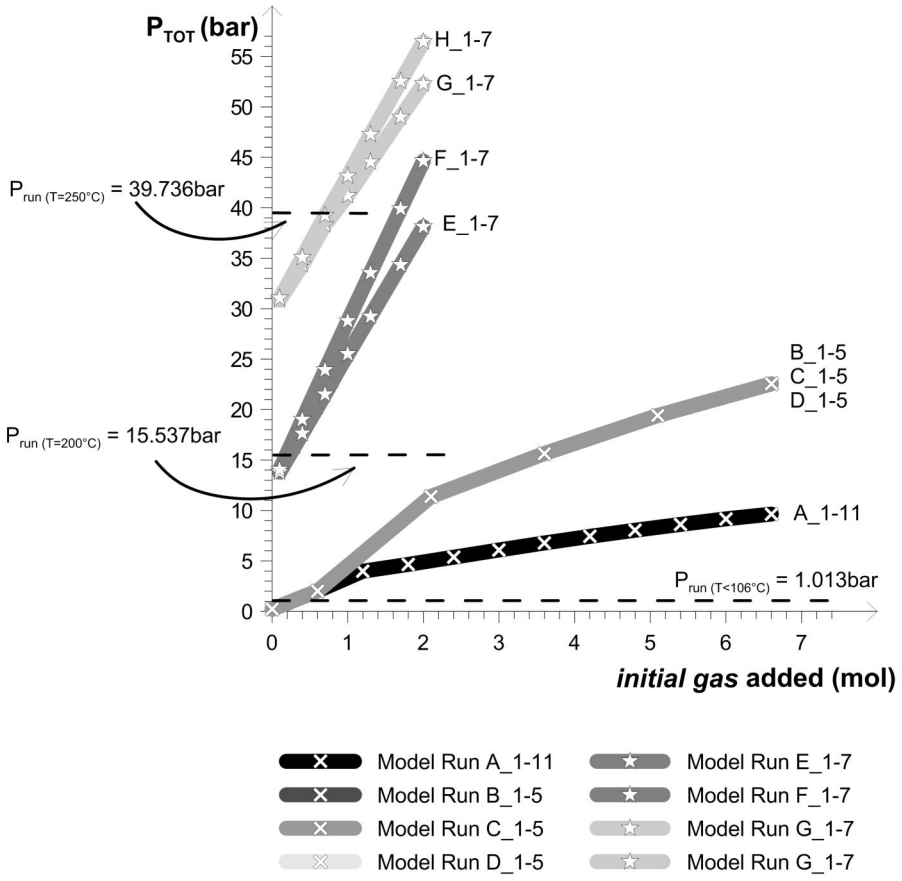
P_TOT (bar)
55
50
45
40
35
30
25
20
15
10
5
0
0
1
2
3
4
5
6
7
initial gas added (mol)
H_1-7
G_1-7
F_1-7
E_1-7
B_1-5
C_1-5
D_1-5
A_1-11
P run (T=250°C) = 39.736bar
P run (T=200°C) = 15.537bar
P run (T<106°C) = 1.013bar
Model Run A_1-11
Model Run B_1-5
Model Run C_1-5
Model Run D_1-5
Model Run E_1-7
Model Run F_1-7
Model Run G_1-7
Model Run G_1-7

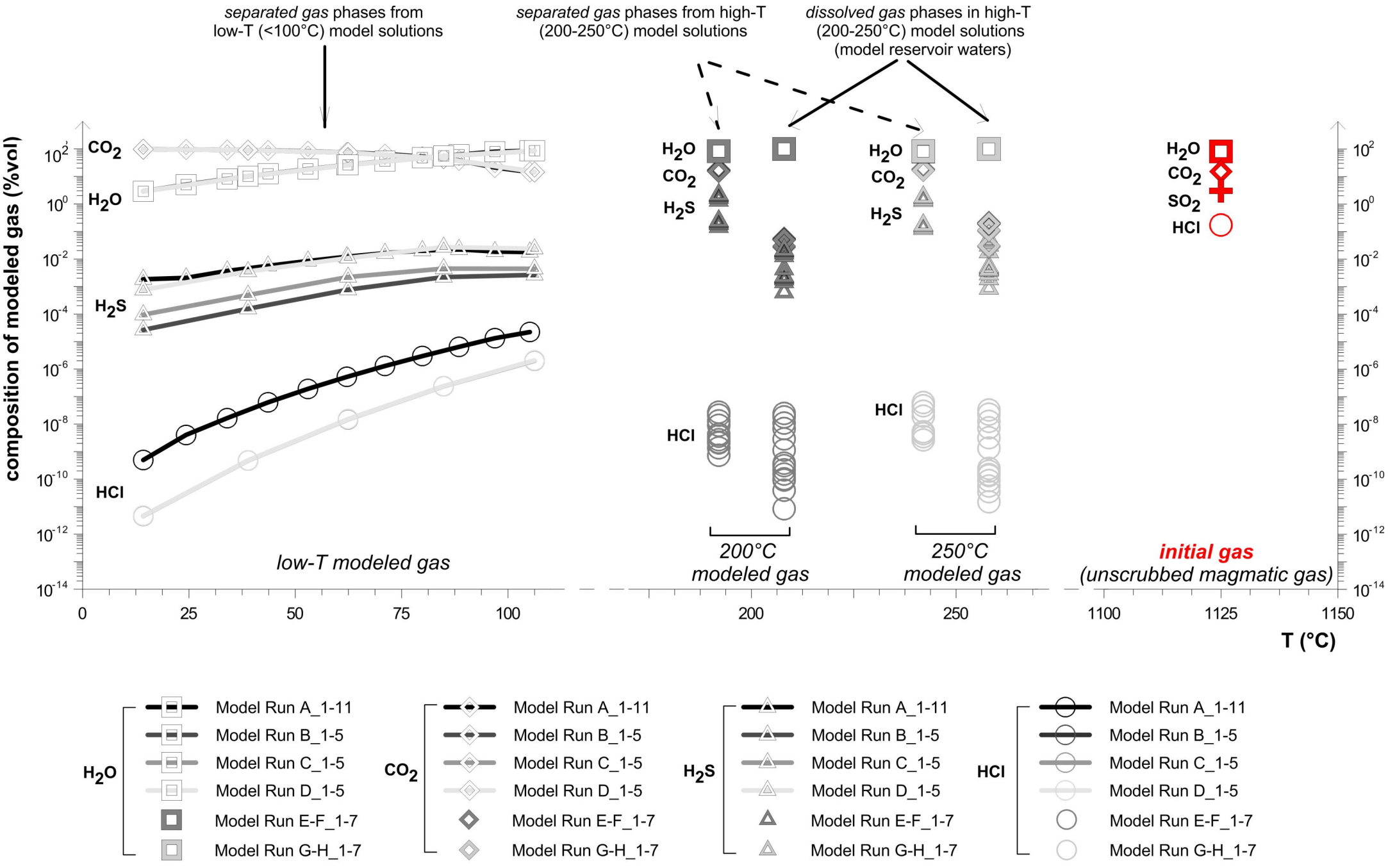
separated gas phases from low-T (<100°C) model solutions
separated gas phases from high-T (200-250°C) model solutions
dissolved gas phases in high-T (200-250°C) model solutions (model reservoir waters)
composition of modeled gas (%vol)
CO2
H2O
H2S
HCl
SO2
low-T modeled gas
200°C modeled gas
250°C modeled gas
initial gas
(unscrubbed magmatic gas)
T (°C)
Model Run A_1-11
Model Run B_1-5
Model Run C_1-5
Model Run D_1-5
Model Run E-F_1-7
Model Run G-H_1-7

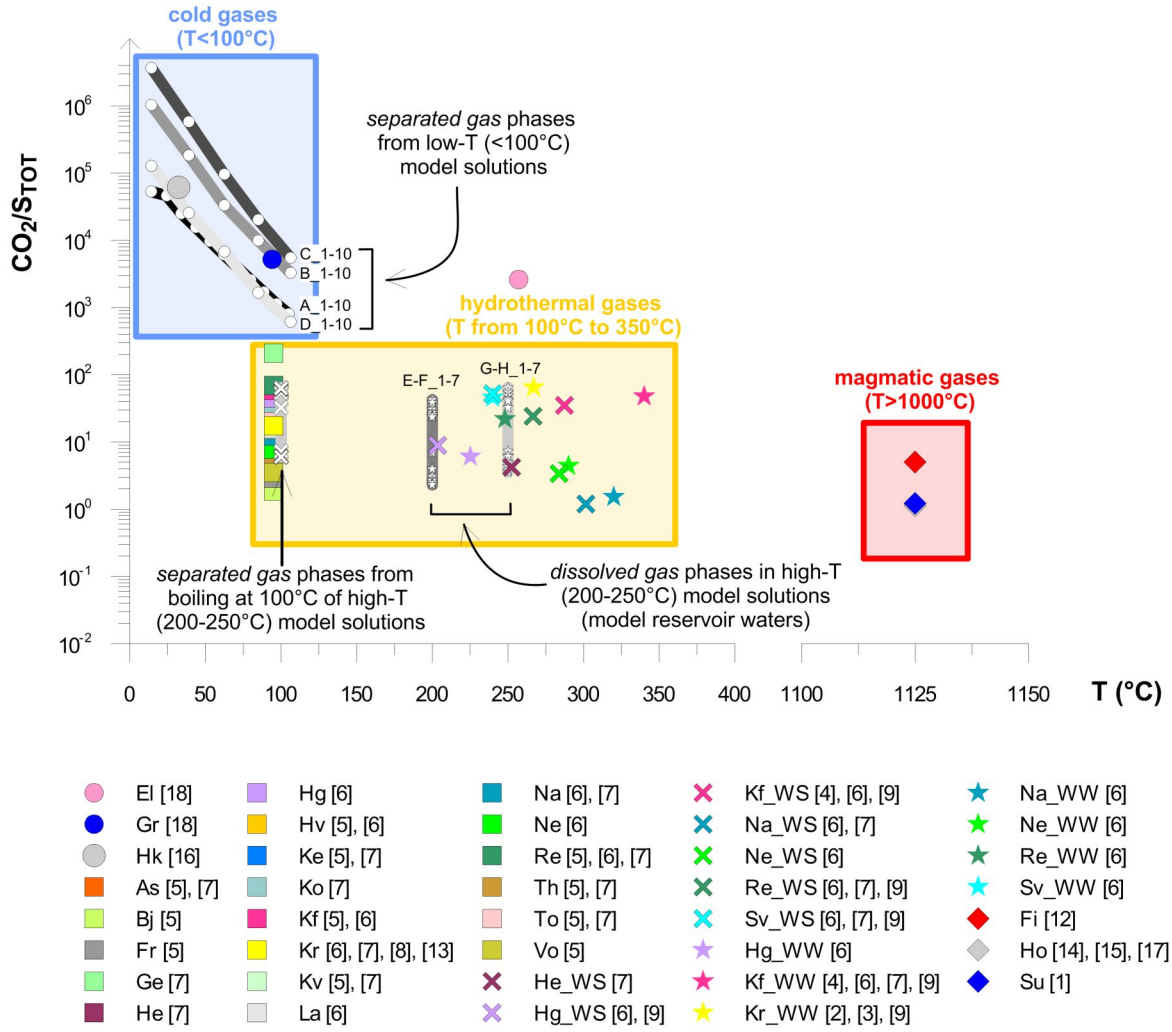
cold gases
(T<100°C)
separated gas phases
from low-T (<100°C)
model solutions
C_1-10
B_1-10
A_1-10
D_1-10
hydrothermal gases
(T from 100°C to 350°C)
E-F_1-7
G-H_1-7
magmatic gases
(T>1000°C)
separated gas phases from
boiling at 100°C of high-T
(200-250°C) model solutions
dissolved gas phases in high-T
(200-250°C) model solutions
(model reservoir waters)
CO2/STOT
T (°C)
El [18]
Gr [18]
Hk [16]
As [5], [7]
Bj [5]
Fr [5]
Ge [7]
He [7]
Hg [6]
Hv [5], [6]
Ke [5], [7]
Ko [7]
Kf [5], [6]
Kr [6], [7], [8], [13]
Kv [5], [7]
La [6]
Na [6], [7]
Ne [6]
Re [5], [6], [7]
Th [5], [7]
To [5], [7]
Vo [5]
He_WS [7]
Hg_WS [6], [9]
Kf_WS [4], [6], [9]
Na_WS [6], [7]
Ne_WS [6]
Re_WS [6], [7], [9]
Sv_WS [6], [7], [9]
Hg_WW [6]
Kf_WW [4], [6], [7], [9]
Kr_WW [2], [3], [9]
Na_WW [6]
Ne_WW [6]
Re_WW [6]
Sv_WW [6]
Fi [12]
Ho [14], [15], [17]
Su [1]

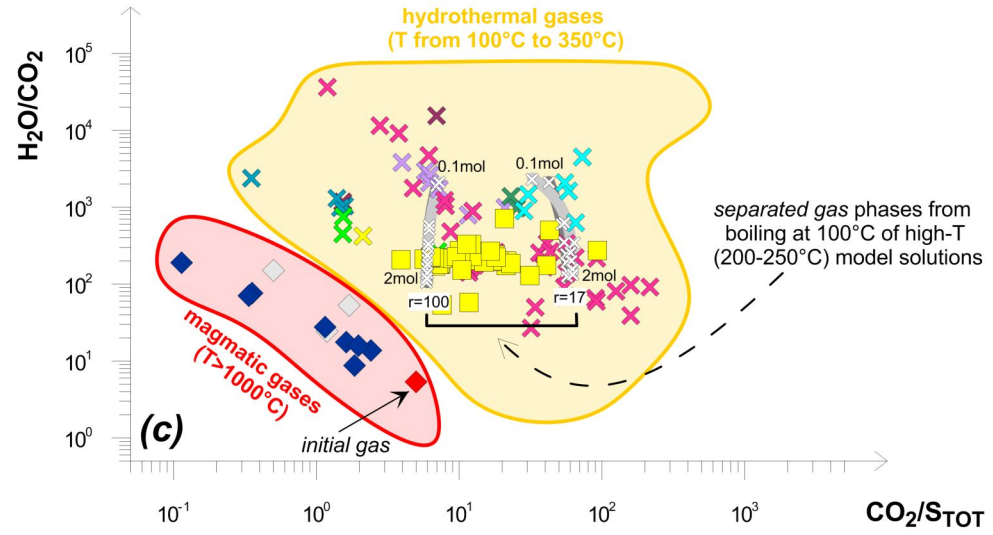

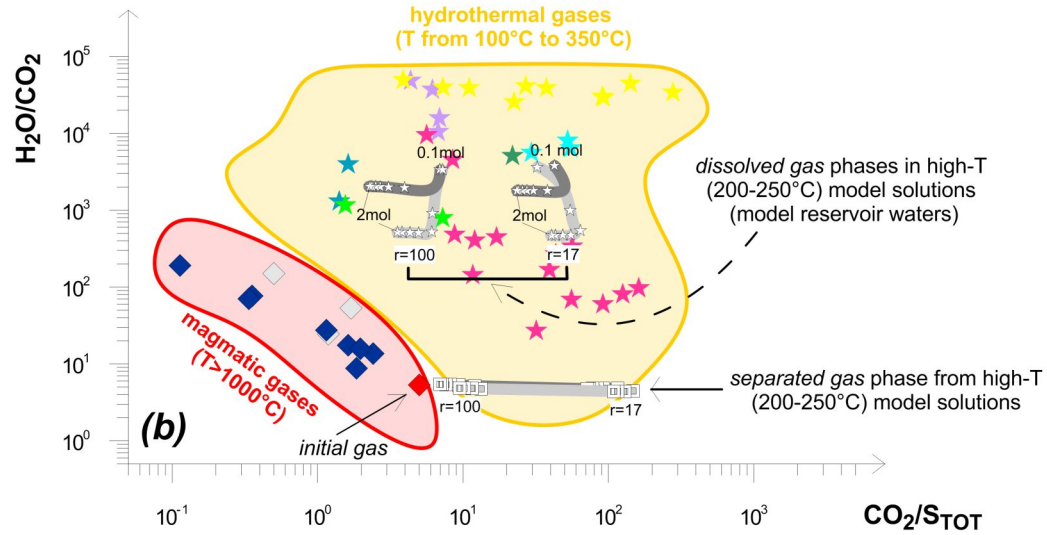

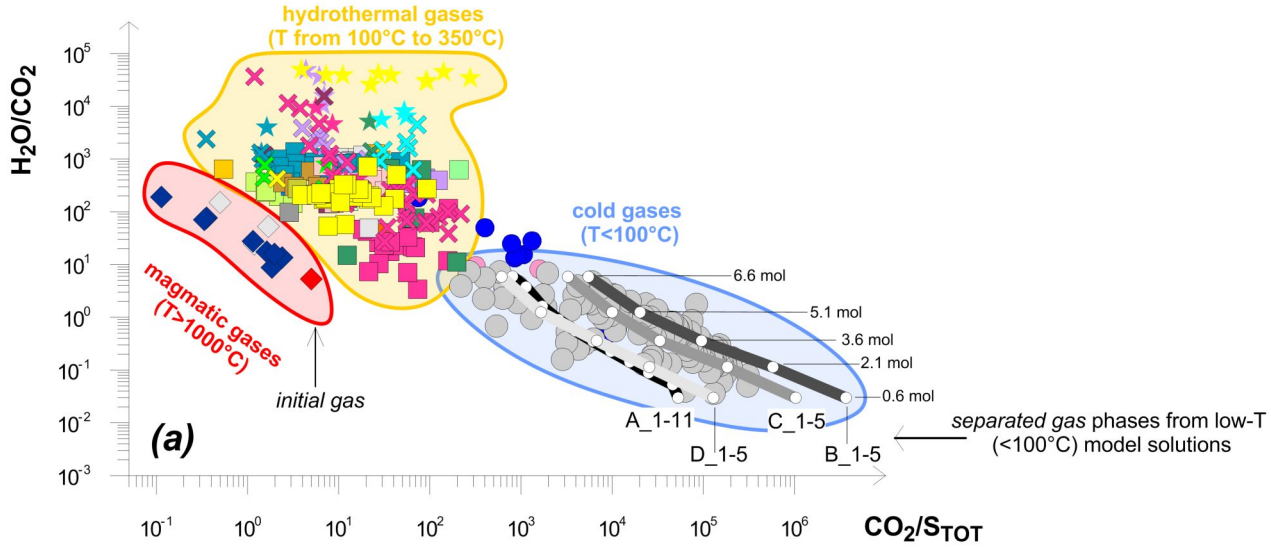

El [18]
Gr [18]
Hk [16]
As [5], [7]
Bj [5]
Fr [5]
Ge [7]
He [7]
Hg [6]
Hv [5], [6]
Ke [5], [7]
Ko [7]
Kf [5], [6]
Kr [6], [7], [8], [13]
Kv [5], [7]
La [6]
Na [6], [7]
Ne [6]
Re [5], [6], [7]
Th [5], [7]
To [5], [7]
Vo [5]
He_WS [7]
Hg_WS [6], [9]
Kf_WS [4], [6], [9]
Kr_WS [11]
Na_WS [6], [7]
Ne_WS [6]
Re_WS [6], [7], [9]
Sv_WS [6], [7], [9]
Hg_WW [6]
Kf_WW [4], [6], [7], [9]
Kr_WW [2], [3], [9]
Na_WW [6]
Ne_WW [6]
Re_WW [6]
Sv_WW [6]
Fi [12]
Ho [14], [15], [17]
Su [1]
Model Run A_1-11
Model Run B_1-5
Model Run C_1-5
Model Run D_1-5
Model Run E-F_1-7
Model Run G-H_1-7
Model Run E-F_1-7
Model Run G-H_1-7
Model Run E-F_1-7
Model Run G-H_1-7

Table A.1: Kinetic parameters introduced in EQ6 input file for gas and solid reactants. These parameters control the dissolution-precipitation reactions occurring along the reaction path in a gas-water-rock system. See Appendix A for details.

reactants	**entered in EQ6 input file as:**	**dissolution rate**	**dissolution rate constant (k; mol·cm^{-2}·s^{-1})**	**apparent activation energy (E_a; kcal·mol^{-1})**	**BET specific surface area (A_{BET}; cm^2/g)**	**total surface area (s; cm^2)**
Initial gas	gas reactant	relative rate 1-100[(1)]				
Hyd-Hekla-glass	solid reactant	TST rate law	$8.56 \cdot 10^{-11}$ (at 25°C)	6.09 (at 25°C)	1200	$7.81 \cdot 10^{6}$
Hekla-glass-cations	special reactant	relative rate 1[(2)]		-		
Hyd-Krýsuvík-glass	solid reactant	TST rate law	$8.56 \cdot 10^{-11}$ (at 25°C)	6.09 (at 25°C)	1400	$3.44 \cdot 10^{7}$
Krýsuvík-glass-cations	special reactant	relative rate 1[(3)]		-		

[(1)] dissolution rate relative to *Hyd- Hekla or Krýsuvík-glass* rate; [(2)] and [(3)] are dissolution rates relative to *Hyd-Hekla-glass* rate and *Hyd-Krýsuvík-glass* rate, respectively.

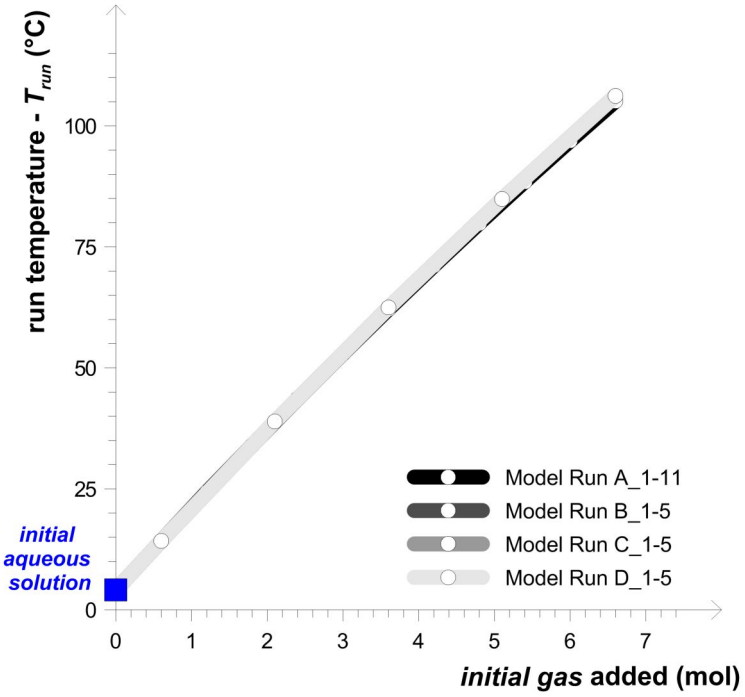
run temperature - T_{run} (°C)
100
75
50
25
0
initial aqueous solution
0
1
2
3
4
5
6
7
initial gas added (mol)
Model Run A_1-11
Model Run B_1-5
Model Run C_1-5
Model Run D_1-5